IEEE Access
Multidisciplinary ⋮ Rapid Review ⋮ Open Access Journal

Received 9 January 2023, accepted 25 January 2023, date of publication 2 February 2023, date of current version 8 February 2023.

Digital Object Identifier 10.1109/ACCESS.2023.3241611

RESEARCH ARTICLE

Drivers' Warning Application Through Personalized DSSS-CDMA Data Transmission by Using the FM Radio Broadcasting Infrastructure

RADU GABRIEL BOZOMITU[1], (Member, IEEE), AND FLORIN DORU HUTU[2], (Senior Member, IEEE)

[1]Faculty of Electronics, Telecommunications and Information Technology, "Gheorghe Asachi" Technical University of Iaşi, 700050 Iaşi, Romania
[2]Univ Lyon, INSA Lyon, Inria, CITI, EA3720, 69621 Villeurbanne, France

Corresponding author: Radu Gabriel Bozomitu (bozomitu@etti.tuiasi.ro)

ABSTRACT In this paper, a new drivers' warning application through personalized Direct-Sequence Spread Spectrum Code-Division Multiple Access (DSSS-CDMA) transmissions, performed using the FM radio broadcasting infrastructure is presented. The proposed application is designed to simultaneously transmit a maximum of 15 low-resolution image notifications together with standard FM radio broadcasting in different geographical areas. The application is intended to warn drivers of significant driving events in major traffic areas of a country. The proposed solution is low-cost and rapid to put into practice because the modifications, both on the transmission infrastructure and on the receiver's side, are relatively easy to implement. The transmission of image notifications is performed in subsidiary bands of commercial FM radio systems. The receiver is implemented using the Software-Defined Radio (SDR) paradigm and is able to extract the audio signal (corresponding to the usual FM transmission) and the data component, depending on the geographical area in which the vehicle is located. The receiver is based on a novel implementation of a modified Costas loop using two new nonlinear limiters. Appropriate image notification is selected using a specific decoding key, generated according to the geographical position of the vehicle. The performance of the data transmission system is analyzed by plotting the Bit Error Rate (BER) versus the signal-to-noise ratio of the data signal for different numbers of image notifications simultaneously transmitted. The proposed radio communication system was validated through an experimental setup based on Universal Software Radio Peripheral (USRP) devices driven by MATLAB/Simulink software.

INDEX TERMS Automotive applications, digital modulation, radio broadcasting, radio communication, software defined radio.

I. INTRODUCTION

As shown by numerous European Community and World Health Organization (WHO) reports, road accidents are one of the leading causes of death worldwide. According to recent WHO reports [1], road injuries are among the top ten causes of death in low-income, lower-middle-income, and upper-middle-income countries. In the European Union (EU), regarding the number of fatalities per million inhabitants between 2010 and 2020, Romania occupied an undesirable first place with 117 and 85 deaths, respectively [2]. These values are approximately twice the European average, which between the aforementioned years is 67 and 42, respectively [2]. In France, a country that is representative of the EU situation, in 2010 and 2020, the number of fatalities per million inhabitants was 64 and 39, respectively, which is very close to the average of the European Union. The situation is even worrying in African countries where, in 2018, the WHO reported 26.6 deaths in traffic accidents per 100000 inhabitants, a number that is almost three times higher than the one corresponding to the average of the European countries [3].

The associate editor coordinating the review of this manuscript and approving it for publication was Ayaz Ahmad.

This work is licensed under a Creative Commons Attribution-NonCommercial-NoDerivatives 4.0 License.
For more information, see https://creativecommons.org/licenses/by-nc-nd/4.0/

The main causes of road accidents are speed, not adapted to weather, road, traffic conditions, or above the legal limit, followed by irregular pedestrian crossings and failure to give priority to pedestrians regularly employed in crossing. To these aspects, the state of infrastructure in certain countries, such as Romania, has been added. According to data presented by the European Commission, 52% of road traffic fatalities occur on rural roads, 40% in urban areas, and only 8% in motorways [4]. The low number of deaths caused by motorway accidents is due to the higher degree of safety that highways provide to drivers, as well as the fact that the physical delimitation of driving directions makes frontal collisions almost impossible. In the conditions in which there are too few highways in Romania, traffic is carried out on roads without direction separators, with a single traffic lane, which favors the occurrence of such accidents. Other risk factors that appear on national roads include improperly signposted repair works, road conditions (ex. potholes), less inspired works carried out by the authorities, such as islands located in the middle of the road, and the state of fatigue of drivers. The significant increase in car parks in recent years in certain countries has also determined the excessive usage of existing infrastructure, which determines the increase in road accidents.

In recent years, there has been an improvement in traffic safety due to actions taken in European countries. However, due to the complexity of traffic events and their dynamic nature, progress in road safety is quite slow. The actions taken to increase traffic safety must involve the roadway environment, vehicles, and road users. The most significant academic research has been presented in the literature regarding road markings as an important road safety element [5]. A modern concept, which encourages drivers to naturally adopt a behavior consistent with the road design, is the ''self-explaining roads'' concept, which was first implemented in the Netherlands [6].

In addition to safety measures regarding road infrastructure, a series of safety features and different modules for Advanced Driver Assistance System (ADAS) have been installed on all modern cars [7].

Moreover, the European Commission has officially launched the United Nations' Global Plan, which sets out how to achieve the target of reducing road traffic deaths and injuries by 50% by 2030 [8]. This plan reinforces the EU's own aspirations, which aims to halve the number of fatalities and serious injuries on European roads by 2030 as a milestone on the way to 'Vision Zero' – zero fatalities and serious injuries by 2050 [8].

To meet this goal, this paper proposes a new warning system for drivers through visual notifications transmitted simultaneously in a maximum of 15 distinct regions of a country using the existing FM infrastructure. Compared to the application introduced by the authors in [9], the radio communication system proposed in this study is more complex, performing the simultaneous warning of drivers, placed in 15 different regions of a county, about different traffic events, using the same broadcasting infrastructure.

Other types of radio access technologies, such as cellular vehicle-to-everything C-V2X and dedicated short-range communication (DSRC), are envisaged to improve traffic safety [10]. As is known, for the implementation of this type of vehicular communication, a complex and expensive infrastructure based on the Internet is required. Therefore, the implementation of such a system requires a fairly long period of time. However, road infrastructure in European countries is increasing, and the implementation of measures to increase road safety has become a stringent necessity. Thus, the proposed driver's warning system, based on Direct-Sequence Spread Spectrum Code-Division Multiple Access (DSSS-CDMA) transmission [11], [12], [13], [14], [15], [16], can be an alternative to these complex and expensive communication systems, benefiting from the existing FM broadcasting infrastructure.

Initially employed in a large number of military and satellite communications, DSSS modulation techniques, and more generally, spread spectrum communications, were adopted by civil applications due to their relatively low power transmission and robustness to channel degradation (fading, multipaths, impulsive noise, etc.) [17]. Moreover, this modulation technique allows different users to share the same communication channel simultaneously using individual orthogonal sequences.

Many applications of this modulation technique or its variations have been encountered. Indeed, the DSSS is found in the IEEE 802.11b standard, and it has also been employed in various positioning systems (GPS, Galileo, or Glonass). Another standard based on DSSS is the 802.15.4 physical layer, and more recently, LoRa also applies a proprietary spread spectrum modulation. Indeed, LoRa is based on chirp spread spectrum modulation, which consists of employing linear frequency-modulated chirp (frequency varying linearly in time) pulses to encode the information to transmit.

DSSS modulation schemes have also been employed in indoor wireless infrared communications to overcome fluorescent light interference and multipath dispersion [18].

Several implementations of DSSS modulation using the SDR paradigm have been reported in literature. For example, in [19], the authors described a DSSS implementation on a GNU Radio Companion dedicated to satellite communications. In [20], the authors reported an implementation for the USRP of a software-defined radio transceiver based on DSSS. The spreading sequence is a chaotic signal whit the same properties as a pseudo-random noise (PN) signal, which is classically employed in commercial communications.

The rest of the paper is organized as follows. Section II presents the description of the proposed drivers' warning application through personalized data transmission. This section also presents the implementation of the SDR communication system employed for data transmission by using DSSS-CDMA modulation on typical FM radio

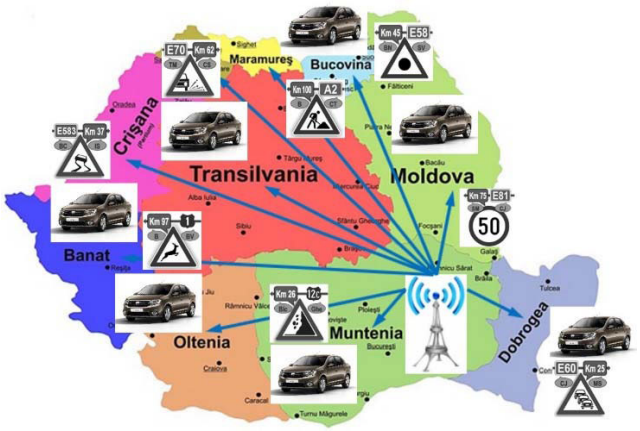

FIGURE 1. Example of the proposed system deployment based on DSSS-CDMA transmission by using the FM radio infrastructure which covers the various regions in Romania.

FIGURE 2. Examples of image notifications which may be employed by the proposed drivers' warning application through personalized DSSS-CDMA transmissions.

broadcasting. Section III presents the simulation results performed in MATLAB/Simulink and those experimentally obtained for the proposed radio communication system. In Section IV, the conclusions of this paper are drawn.

II. MATERIAL AND METHODS

A. DESCRIPTION OF THE PROPOSED APPLICATION

In this paper, a new application for drivers' warning through personalized image notifications simultaneously transmitted in different geographic areas is presented. As shown in Fig. 1, the proposed application can simultaneously transmit a number of n different images in n distinct geographical areas using the existing FM radio infrastructure. In this way, each driver is warned only about traffic events that are specific to the area in which they drive the car. The maximum number of images that can be transmitted simultaneously depends on the capacity of the radio communication channel in the subsidiary FM bands, as well as the signal-to-noise ratio of data transmission.

A non-exhaustive list of traffic events signaled by this broadcasting strategy is given here: road conditions, weather conditions, works on public roads, road accidents, railway passing, congestion on public roads, dangerous intersections, dangerous curves, the need to reduce speed, and many others.

More precisely, the driver is warned in advance of these traffic events by image notifications that are displayed on the tablet screen of the vehicle. Most new vehicles are equipped with such displays, and, if applicable, smartphones may be employed instead. These image notifications are designed to be clear, simple, and easy to understand by drivers, without distracting them from driving safely. Therefore, drivers have sufficient time to react to and avoid unwanted road events. Examples of these image notifications are shown in Fig. 2.

The information to be transmitted is provided by the national road authority to an FM radio station, where it is processed to generate the image notifications in the required format for transmission using appropriate software.

Different technical solutions for transmitting data in FM radio have been presented in the literature [9], [21], [22], [23], [24], [25], [26]. Among these, the Radio Broadcast Data System (RBDS) [24] is used in standard FM radio broadcasting to transmit data of social interest with a data rate of only 1187.5 bit/s in the form of a text message, and the Data Radio Channel (DARC) system [25] can provide general information, traffic information, radio paging, and differential GPS data with a data rate of 16 kbit/s.

Compared to these systems, the radio communication system proposed in this paper presents a higher maximum data rate (35.625 kbit/s), corresponding to 15 images transmitted simultaneously together with the standard FM radio broadcasting in different geographical areas, according to the user's needs. Therefore, our system benefits of high FM radio signal quality and wide-area radio FM network. On the other hand, the proposed system is cheaper, more flexible, and easier to implement due to the use of the existing and widespread radio FM infrastructure and software-defined radio paradigm. Moreover, the proposed solution does not require an Internet connection, which may be weak or non-existent in certain hard-to-reach geographical areas (developing countries).

In Fig. 3, the block diagram of the proposed radio communication system, based on a software-defined radio technique, is presented. The image notifications are broadcasted using DSSS-CDMA modulation, together with standard FM transmission.

The customized baseband signal used for a professional radio transmitter includes the multiplex (MPX) stereo component (used for standard FM radio broadcasting) and a set of data images, which are included in a DSSS-CDMA spectrum component that modulates a 76 kHz subcarrier. The spectrum of the composite signal containing the standard MPX component, together with the data components, is illustrated in Fig. 4.

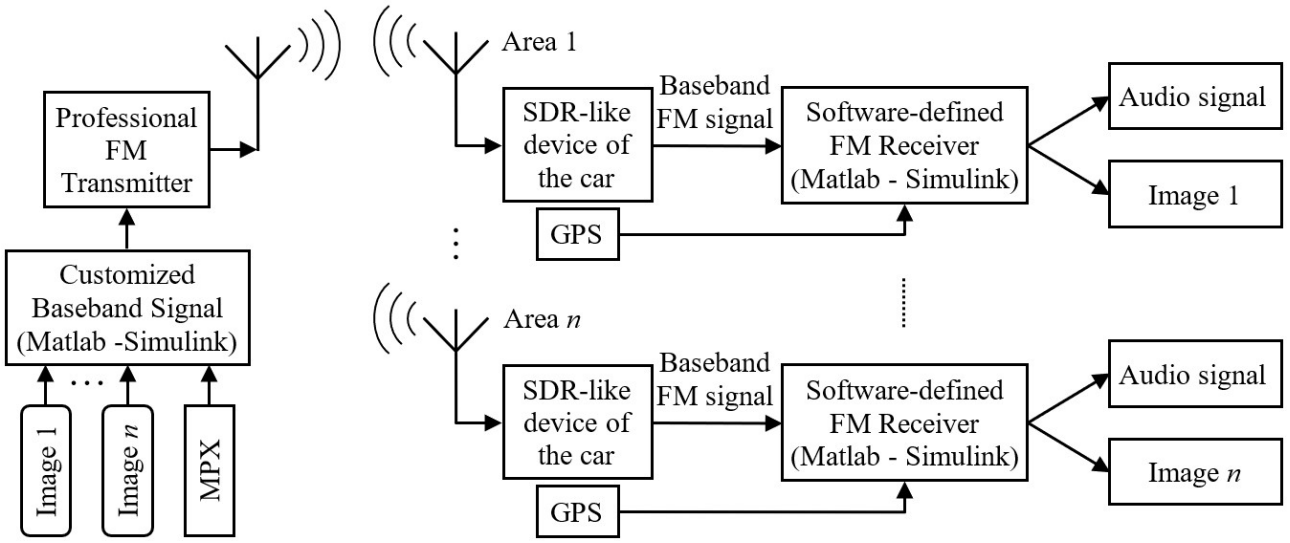

FIGURE 3. Principle of personalized DSSS-CDMA data transmissions on different geographical areas by using the FM radio broadcasting infrastructure.

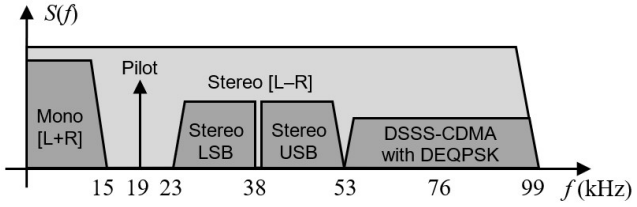

FIGURE 4. Spectrum of the customized baseband signal including the MPX stereo and DSSS-CDMA data signals.

To generalize the problem of image transmission in the FM subsidiary band, the case of n simultaneously transmitted images is considered. However, for practical implementation, n is considered to be equal to 15.

The car's radio receiver is implemented using a software-defined radio technique and is used to receive warning image notifications, according to the geographical position of the car, together with the standard FM transmission.

The implementation of the system using software-defined radio technology offers the following advantages over other similar systems:

- The radio receiver is implemented through software, is flexible, easy to adapt to any changes that may occur in the implementation process, easy to install on the car's tablet, and easy to use by drivers.

- The DSSS-CDMA modulation technique used by the proposed radio communication system can be implemented using software, but the system can be easily reconfigured to any type of modulation by modifying only the software and maintaining the same hardware components.

- The pictograms used to warn drivers about road events transmit a large amount of information without distracting them from the attention necessary to drive the vehicle safely.

B. PROPOSED ARCHITECTURE OF THE FM RADIO TRANSMITTER EMPLOYED FOR FM BROADCATING AND DATA TRANSMISSION

In Fig. 5, the block diagram of the radio transmitter, including the MPX stereo signal and DSSS-CDMA data generators, is illustrated. This customized baseband signal is software-generated using MATLAB/Simulink and is applied to an FM modulator, resulting in a signal with a bandwidth of 200 kHz. This signal is broadcasted by a national FM radio station.

The RF signal is received by software-defined FM radio receivers installed in vehicles located in distinct geographical areas of the country. A certain image is selected using a decoding key specific to the geographical area in which the vehicle is located. This decoding key is generated according to the geographical coordinates of the vehicle position provided by the GPS system or a mobile phone service. The hardware component of the car radio receiver is represented by an SDR-like device (RTL-SDR dongle, as implemented in [27], or a USRP device), which provides the baseband FM modulated signal to the software program.

DSSS-CDMA is a technique in which the different narrowband signals are multiplied by wideband codes, and the codes are orthogonal to each other. Some of the common orthogonal spreading codes used in CDMA systems are the PN sequences, Walsh, and Gold code [16].

In the proposed system, we used long-spreading pseudo-random noise sequences, which were generated using maximum-length shift registers. In already-deployed CDMA systems, PN code sequences are mainly used for code spreading, code scrambling, and code division [28]. For example, code division by PN code offset is used in the IS-95 system [29]. For any single user, the coded messages of the remaining users appear as noise in the received signal. To decode a message, the receiver must already know the

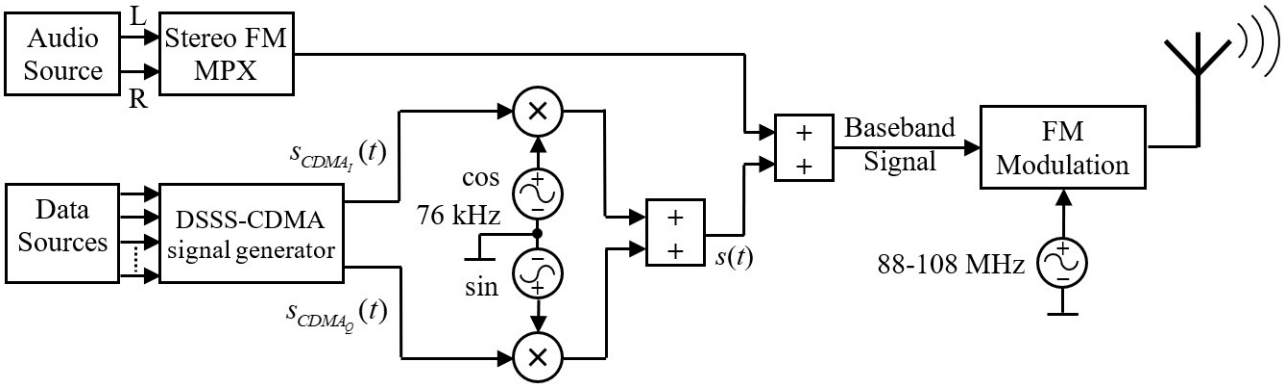

FIGURE 5. Block diagram of the transmitter including the MPX stereo signal and DSSS-CDMA data generators.

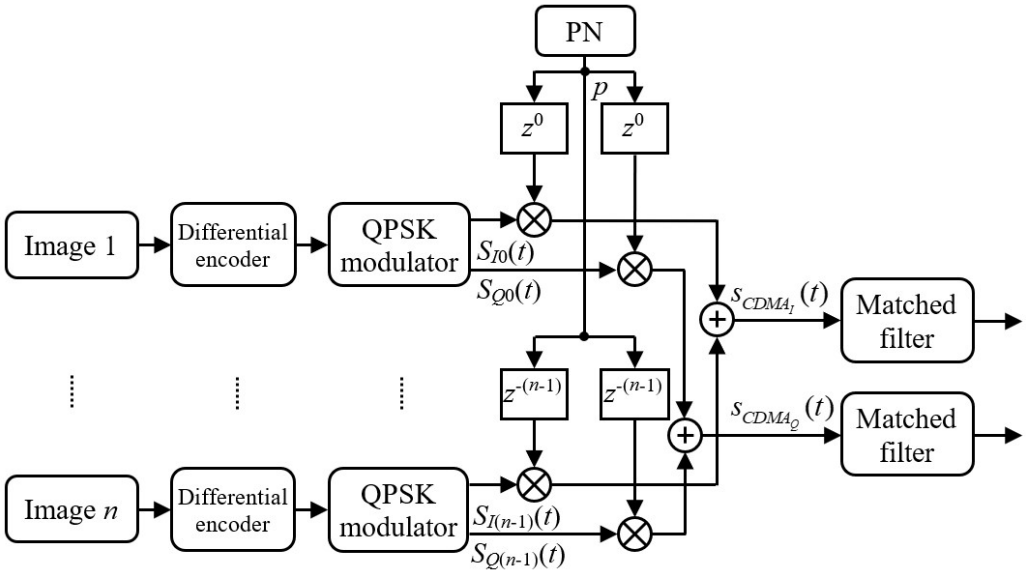

FIGURE 6. Block diagram of the proposed DSSS-CDMA signal generator.

spreading code employed at the transmission (the decoding key).

A detailed block diagram of the direct-sequence spread spectrum generator proposed in our application is presented in Fig. 6. The DSSS-CDMA technique used in the proposed application enables the simultaneous transmission of a relatively large number of images in the same frequency band of a radio channel and consequently increases the channel capacity. In the case of the proposed application, synchronization of the transmitted data sequences can be easily performed using software at the transmitter stage.

First, the data images are differentially encoded; then, in order to increase the speed of data transmission, the QPSK modulation is used. Using QPSK modulation with differential encoding (DEQPSK) [30], the resulting signal is not affected by a fixed phase offset introduced by the lack of phase synchronization between the transmitter and receiver [31]. Thus, the symbol rate of the DEQPSK signal is given by

$$f_s = f_b/2 \tag{1}$$

where f_b is the input data rate of each transmitted image.

To implement a DSSS-CDMA communication system, a pseudo noise spreading code (PN) was used to spread the DEQPSK data samples (Fig. 6).

The PN codes employed in the proposed system are generated with $\log_2(n+1)$ shift registers (by using a primitive polynomial of degree N [32], [33]) with linear feedback, having a length $n = 2^N - 1$, which represents the maximum number of users (images transmitted simultaneously), and having a chip rate $f_{ch} = 19$ kHz (the chip duration is $T_0 = 1/f_{ch}$). The value of the chip rate is limited by the available bandwidth of the communication channel in the subsidiary FM bands, which is between 53 and 99 kHz. Thus, n different pseudo-random orthogonal sequences are cyclically shifted. The symbol

rate (f_s) used in the proposed system is chosen such that the chip rate is an integer multiple of the input symbol rate according to the following relation:

$$f_{ch} = (n+1) \cdot f_s \tag{2}$$

where $SF = n + 1$ represents the spreading factor of the proposed DSSS-CDMA transmission.

According to (2), the number of images transmitted simultaneously (which represents the length of the PN code) is given by

$$n = (f_{ch}/f_s) - 1 \tag{3}$$

Table 1 lists the number of images that can be transmitted simultaneously for different values of input data rate.

TABLE 1. Number of images that can be transmitted simultaneously for different values of the input data rate.

Data rate of each image (f_b) [bit/s]	Symbol rate of each DEQPSK image (f_s) [symbol/s]	Spreading factor (SF)	Number of simultaneously transmitted images (n)	System data rate for n images (f_n) [kbit/s]
4750	2375	8	7	33.250
2375	1187.5	16	15	35.625
1187.5	593.75	32	31	36.8125
593.75	296.875	64	63	37.40625

The value of the symbol rate (f_s) used in the proposed application was chosen to be identical to the data rate of the RBDS signal from standard FM transmissions, which is equal to 1187.5 bit/s. Thus, the input data rate of each image used in the proposed radio communication system is $f_b = 2375$ bit/s, which allows simultaneous transmission of $n = 15$ images. Thus, the maximum data rate provided by the proposed system for all 15 images transmitted simultaneously is 35.625 kbit/s. In the design of the system, a trade-off must be made between the data rate and the BER of the data signal with DSSS-CDMA modulation because the transmission of a larger amount of data causes a significant increase in the noise on the communication channel due to a larger number of users (simultaneously transmitted images), thus increasing the BER. Therefore, a number of more than 31 images transmitted simultaneously is not convenient for the proposed application, due to a very low data rate of each transmitted image and the significant decrease of the signal-to-noise ratio (SNR).

According to Fig. 6, after DEQPSK modulation, the real and imaginary parts of the resulting signals are multiplied by PN sequences obtained from a unique PN sequence (p) of length 15, which is cyclically shifted. To increase the symmetry of the problem and improve loop synchronization, we used the same pseudo-noise sequence for both signal paths. In this manner, the preamble bits of the input data sequence (images) used for synchronization will be identical for both data sequences on the two channels (in-phase - I and quadrature - Q), which will improve signal detection. The resulting spread sequences are then added together on each signal path to obtain two corresponding DSSS-CDMA sequences.

The DEQPSK signals can be written as:

$$s_{DEQPSK_j}(t) = S_{Ij}(t) + j \cdot S_{Qj}(t), \quad j = 0, 1, \ldots, n-1 \tag{4}$$

where

$$\begin{cases} S_{Ij}(t) = \mathrm{Re}\left\{s_{DEQPSK_j}(t)\right\} \\ S_{Qj}(t) = \mathrm{Im}\left\{s_{DEQPSK_j}(t)\right\}, \end{cases} \quad j = 0, 1, \ldots, n-1 \tag{5}$$

are the coordinates of the message points of each DEQPSK signal with the values "$\pm a$" over the entire cycle of the PN sequence. The sampling rate employed in the proposed software-defined radio communication system was 228 kHz, and the coordinates of the message points were $a = 50$ mV.

Thus, for the DEQPSK signal, we can write:

$$S_{Ij}^2(t) + S_{Qj}^2(t) = 2a^2, \quad j = 0, 1, \ldots, n-1 \tag{6}$$

For the time taken to complete one cycle for the PN sequence ($n \cdot T_0$), in which the coordinates of the message points of the DEQPSK signal have constant values in time (S_{Ij} and S_{Qj}), the two DSSS-CDMA sequences on the two signal paths (I and Q) can be written as

$$\begin{cases} \boldsymbol{s_{CDMA_I}}[kT_0] = \sum_{j=0}^{n-1} S_{Ij} \cdot \boldsymbol{p_j}[kT_0] \\ \boldsymbol{s_{CDMA_Q}}[kT_0] = \sum_{j=0}^{n-1} S_{Qj} \cdot \boldsymbol{p_j}[kT_0], \end{cases} \quad k = 0, 1, \ldots, n-1 \tag{7}$$

where $\boldsymbol{s_{CDMA_I}}$, $\boldsymbol{s_{CDMA_Q}}$, and $\boldsymbol{p_j}$ are n-dimensional vectors. The elements of the vectors $\boldsymbol{s_{CDMA_I}}$, $\boldsymbol{s_{CDMA_Q}}$ represent the values of the signals $s_{CDMA_I}(t)$, $s_{CDMA_Q}(t)$ at times that are multiples of chip duration ($k \cdot T_0$, $k = 1, 2, \ldots$).

In equation (7), the vectors $\boldsymbol{p_j}$ are the cyclic shifted versions by j terms of the pseudo-random noise sequence [32], having $n = 15$ elements given by

$$\boldsymbol{p_j} = \begin{bmatrix} b_j & b_{(j+1)} & \cdots & b_{(n-1)} & b_0 & \cdots & b_{(j-1)} \end{bmatrix}, \quad j = 0, 1, \ldots, n-1 \tag{8}$$

After passing through the matched filters, the two DSSS-CDMA sequences from (7) modulates via complex modulation a 76 kHz subcarrier (the fourth harmonic of the pilot tone), and the following signal is generated:

$$s(t) = s_{CDMA_I}(t)\sin(2\pi f_c t + \theta) + s_{CDMA_Q}(t)\cos(2\pi f_c t + \theta) \tag{9}$$

where $f_c = 76$ kHz is the subcarrier frequency and θ is its initial phase.

Due to the overlapping of the maximum $n = 15$ pairs of the DSSS-CDMA signals, the constellation of the resulting signal is similar to the constellation of an M-QAM signal, whose message points are pseudo-randomly generated. This signal consists of n overlapping images, and its number of levels, L is

$$L = \sqrt{M} = n + 1 \tag{10}$$

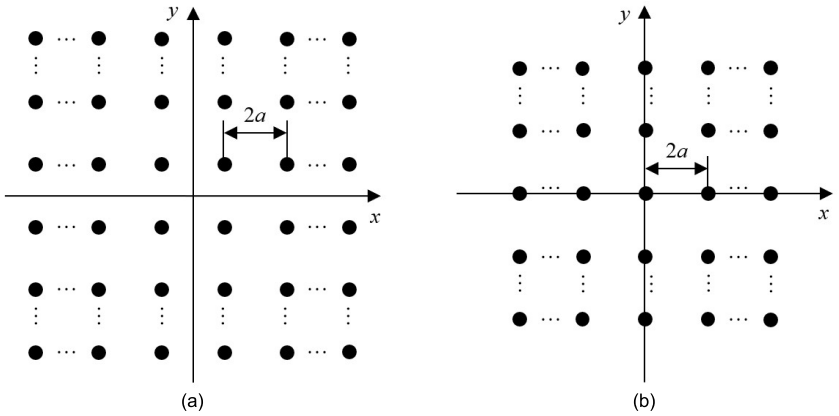

FIGURE 7. Constellations of the generated signals: a) for an odd number of images transmitted simultaneously; b) for an even number of images transmitted simultaneously.

Thus, for 15 images transmitted simultaneously, the two obtained DSSS-CDMA sequences have 16 levels (8 positive and 8 negative). For an odd number of images transmitted simultaneously, the constellation of the resulting signal is of the form illustrated in Fig. 7 (a), whereas for an even number of transmitted images, the constellation of the resulting signal has the shape shown in Fig. 7 (b). For $n = 1, 3, 7$, and 15 images transmitted simultaneously, square constellations were obtained, which were similar to the constellations of the 4-QAM, 16-QAM, 64-QAM, and 256-QAM signals, respectively. Non-square constellations were generated for all other situations. In Fig. 7, $2a$ represents the minimum Euclidean distance between any pair of symbols in the signal constellation.

According to the Policy Statement adopted by the Federal Communication Commission no. 22 Record [34], during stereophonic transmissions, multiplex subcarriers and their significant sidebands must be within the range of 53 – 99 kHz. The channel bandwidth required for the transmission of the baseband DSSS-CDMA signals presented in (7) is given by [35]

$$BW = f_{ch}\,(1+\beta)/2 \tag{11}$$

where the roll-off factor β may have different values in the range of (0, 1).

Thus, for the transmission of the RF signal described by (9), the maximum bandwidth required is 38 kHz (twice the baseband bandwidth), which agrees with the available resources for data transmission in the subsidiary FM channel on the 76 kHz subcarrier.

C. IMPLEMENTATION OF THE DEDICATED SOFTWARE DEFINED RADIO RECEIVER

The most sensitive part of a DSSS system is the synchronization of the PN sequence of the transmitter with that generated at the receiver stage. Synchronization can be implemented using a known preamble between the transmitter and receiver, which is synchronized by a matched filter [36], [37]. In the literature, this method is known as Data-Aided (DA) synchronization [38]. In order to perform synchronization, several other techniques, such as single dwell serial search (SDSS), multiple dwell serial search, and matched filter correlations have also been presented. In this paper, a synchronization technique based on SDSS was employed to despread the DSSS-CDMA signal.

In Fig. 8, the block diagram of the Simulink-based FM radio receiver, including the audio stereo signal decoder and DSSS-CDMA demodulator, is presented. The demodulation of the FM signal is performed by a classical non-coherent method based on a Complex Delay Line Frequency Discriminator (CDLFD), as presented in [26]. After FM demodulation, the MPX signal and the DSSS-CDMA signal around the subcarrier frequency of 76 kHz are separated from each other using a low-pass filter (LPF) and a band-pass filter (BPF), respectively. The audio stereo signal is extracted from the MPX signal by using a stereo FM demultiplexer, a stereo decoder and a de-emphasis stage as presented in ''RTL-SDR book library'' [26].

To extract the two CDMA sequences from the received signal, a synchronous detector based on the Costas loop, which ensures phase synchronization between the transmitted and recovered carriers at a frequency of 76 kHz (the fourth harmonic of the pilot tone), is used. The recovered quadrature carrier was built by multiplying the 19 kHz frequency of the pilot tone provided by the phase lock loop (PLL) circuit used in the Stereo FM demultiplexer stage.

To extract a certain image from the two received DSSS-CDMA signals, a PN sequence was locally generated in the receiver stage, by using the DLL-based stage in Fig. 8. The spreading codes of cyclically shifted PN sequences depend on the geographical area in which the vehicle finds itself at a given time. After despreading the DSSS-CDMA signal using a DLL-based stage, demodulation of the resulting baseband DEQPSK signal is performed, and the desired image (corresponding to a certain decoding key) is reconstructed.

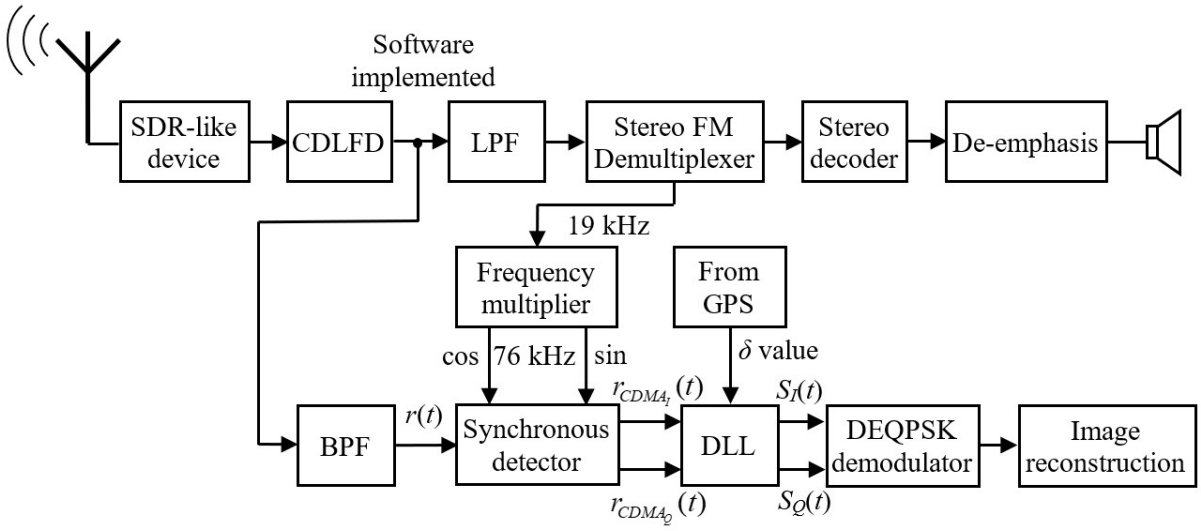

FIGURE 8. Block diagram of the Simulink-based FM radio receiver including audio signal demodulator and DSSS-CDMA decoder.

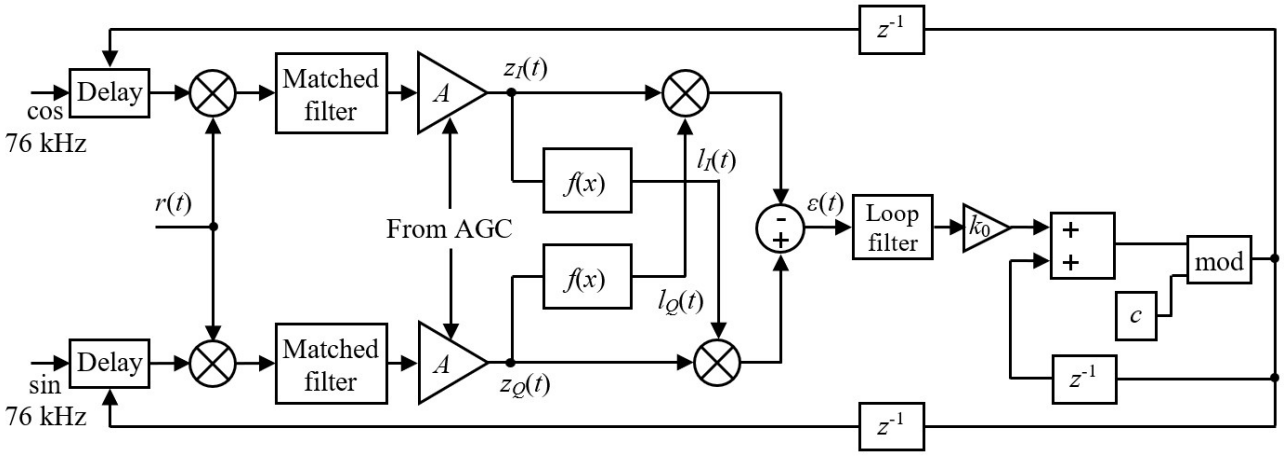

FIGURE 9. Synchronous detector based on modified Costas loop with nonlinear limiters.

1) SYNCHRONOUS DETECTION BASED ON MODIFIED COSTAS LOOP

To perform the demodulation of the DSSS-CDMA signal given by (9) (which includes the two DSSS-CDMA sequences), a novel implementation of the modified version of a Costas loop [39], [40], [41] with new nonlinear limiters ($f(x)$), illustrated in Fig. 9, has been proposed. As depicted in Fig. 9, the phase correction provided by the Costas loop depends on the loop step, k_0 and the constant $c = 3$, which is the ratio between the sampling frequency (228 kHz) and subcarrier frequency (76 kHz). In this figure, "mod" represents the modulo operation.

For odd numbers of images (max. 15 images) transmitted simultaneously, the limiters used in the Costas loop in Fig. 9 are described by the following function for positive x:

$$f(x) = a\,(2l-1)\,, \quad \text{if } \delta_l < x < \delta_{l+1}; \quad l = 1, 2, \ldots, 8 \tag{12}$$

The decision levels δ_l are defined as follows:

$$\delta_l = \begin{cases} 0, & l = 1 \\ 2a(l-1), & 2 \le l \le 8 \\ \infty, & l > 8 \end{cases} \tag{13}$$

For even numbers of images (max. 14 images) transmitted simultaneously, the limiters used in the proposed version of the Costas loop can be described by the following function:

$$f(x) = 2al, \quad \text{if } \delta_l < x < \delta_{l+1}; \quad l = 0, 1, \ldots, 7 \tag{14}$$

The decision levels δ_l are defined as follows:

$$\delta_l = \begin{cases} a(2l-1), & 0 \le l \le 7 \\ \infty, & l > 7 \end{cases} \tag{15}$$

In Fig. 10, the two nonlinearities described by functions (12) and (14) are represented by blue and red, respectively.

The received DSSS-CDMA signal, at the output of the BPF from Fig. 8 (including two received DSSS-CDMA sequences) can be written as

$$r(t)=r_{CDMA_I}(t)\sin(2\pi f_c t+\theta')+r_{CDMA_Q}(t)\cos(2\pi f_c t+\theta') \tag{16}$$

where f_c is the recovered carrier of 76 kHz, and $r_{CDMA_I}(t)$ and $r_{CDMA_Q}(t)$ are the received multi-level DSSS-CDMA signals at the rate of 19 kHz. The value of θ' is the phase of the recovered subcarrier.

By using the synchronous detector block illustrated in Fig. 9, this signal is multiplied with the quadrature recovered carrier signal of 76 kHz, provided by the PLL (from Stereo FM Demultiplexer stage) and Frequency multiplier stage and after low pass filtering the obtained signals are:

$$\begin{cases} z_I(t) = r_{CDMA_I}(t)\cos\varphi - r_{CDMA_Q}(t)\sin\varphi \\ z_Q(t) = r_{CDMA_I}(t)\sin\varphi + r_{CDMA_Q}(t)\cos\varphi \end{cases} \tag{17}$$

where $\varphi=\theta-\theta'$ is the phase shift between the input and the recovered carrier.

Considering that the phase error is always $|\varphi| < 45°$ [40], [41], the outputs of the two nonlinear limiters in Fig. 9 are:

$$\begin{cases} l_I(t) = r_{CDMA_I}(t) \\ l_Q(t) = r_{CDMA_Q}(t) \end{cases} \tag{18}$$

where, according to Fig. 10,

$$\begin{cases} \max\left[l_{I/Q}(t)\right] = n\cdot a = 15a \\ \min\left[l_{I/Q}(t)\right] = a \end{cases} \tag{19}$$

For small values of φ, the error signal can be written as:

$$\begin{aligned} \varepsilon(t) &= z_Q l_I - z_I l_Q \\ &= r^2_{CDMA_I}(t)\sin\varphi + r_{CDMA_Q}(t)r_{CDMA_I}(t)\cos\varphi \\ &\quad - r_{CDMA_I}(t)r_{CDMA_Q}(t)\cos\varphi + r^2_{CDMA_Q}(t)\sin\varphi \\ &= \left[r^2_{CDMA_I}(t)+r^2_{CDMA_Q}(t)\right]\sin\varphi \\ &\approx \left[r^2_{CDMA_I}(t)+r^2_{CDMA_Q}(t)\right]\varphi \end{aligned} \tag{20}$$

The received signals $r_{CDMA_I}(t)$ and $r_{CDMA_Q}(t)$, provided by the Costas loop, can be described as in (7) and for the time taken to complete one cycle for the PN sequence $(n\cdot T_0)$, these signals can be written as

$$\begin{cases} \boldsymbol{r_{CDMA_I}}[kT_0] = \sum_{j=0}^{n-1} S_{Ij}\cdot \boldsymbol{p_j}[kT_0] \\ \boldsymbol{r_{CDMA_Q}}[kT_0] = \sum_{j=0}^{n-1} S_{Qj}\cdot \boldsymbol{p_j}[kT_0], \end{cases} \quad k=0,1,\ldots,n-1 \tag{21}$$

where $\boldsymbol{r_{CDMA_I}}$ and $\boldsymbol{r_{CDMA_Q}}$ are n-dimensional vectors, and $\boldsymbol{p_j}$ is a cyclically shifted PN sequence, locally generated, of the same form as that from (8).

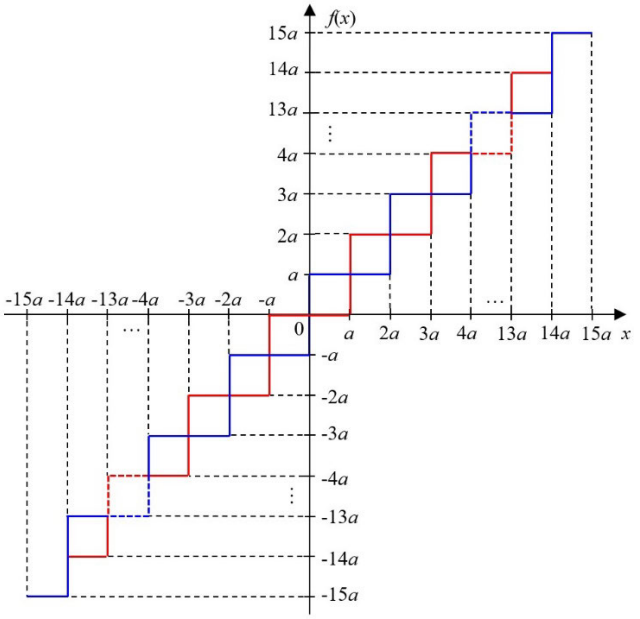

FIGURE 10. Costas loop nonlinearities: a) for an odd number of images (max. 15 images) – blue line; b) for an even number of images (max. 14 images) – red line.

If we note with $\boldsymbol{s_I}$ and $\boldsymbol{s_Q}$ the following n-dimensional vectors, including the coordinates of the message points of the received DEQPSK signal,

$$\begin{cases} \boldsymbol{s_I} = \begin{bmatrix} S_{I0} & S_{I1} & \cdots & S_{I(n-1)} \end{bmatrix} \\ \boldsymbol{s_Q} = \begin{bmatrix} S_{Q0} & S_{Q1} & \cdots & S_{Q(n-1)} \end{bmatrix} \end{cases} \tag{22}$$

then, from (21), after some mathematical manipulation, we obtain:

$$\begin{cases} \boldsymbol{r_{CDMA_I}} = \begin{bmatrix} \boldsymbol{s_I p_0^T} & \boldsymbol{s_I p_1^T} & \cdots & \boldsymbol{s_I p_{(n-1)}^T} \end{bmatrix} \\ \boldsymbol{r_{CDMA_Q}} = \begin{bmatrix} \boldsymbol{s_Q p_0^T} & \boldsymbol{s_Q p_1^T} & \cdots & \boldsymbol{s_Q p_{(n-1)}^T} \end{bmatrix} \end{cases} \tag{23}$$

where $\boldsymbol{p_j^T}$ is the transpose of the vector $\boldsymbol{p_j}$.

If $n=1$ in equation (21) and considering that the elements of the PN sequence $\boldsymbol{p_j}$ can be "±1" and S_{Ij} and S_{Qj} are equal to "$\pm a$", the following equation can be written:

$$S^2_{I0}\boldsymbol{p}_0^2[kT_0] + S^2_{Q0}\boldsymbol{p}_0^2[kT_0] = 2a^2, \quad k=0,1,\ldots,n-1 \tag{24}$$

Since the chipping signal satisfies the condition $p^2(t)=1$, the proposed receiver is able to decode the encoded signal.

Thus, the error signal from (20) for any time that is multiple of chip duration $[kT_0]$ can be written as

$$\varepsilon[kT_0]|_{n=1} = 2a^2\varphi, \quad k=0,1,\ldots,n-1 \tag{25}$$

For $n=15$, according to (19), the minimum and maximum values of the $r^2_{CDMA_I}(t)$ and $r^2_{CDMA_Q}(t)$ signals from (20) vary between a^2 and $225a^2$.

Thus, the error signal from (20), for any time that is a multiple of chip duration $[kT_0]$, varies between a minimum and a maximum value, given by

$$\begin{cases} \varepsilon_{\min}[kT_0] = 2a^2\varphi \\ \varepsilon_{\max}[kT_0] = 450a^2\varphi, \end{cases} \quad k = 0, 1, \ldots, n-1 \qquad (26)$$

Consequently, the circuit in Fig. 9, which is suitable for QPSK signal detection (as illustrated in [41]), can also be used for DSSS-CDMA signal detection.

If the phase error is greater than 45°, the loop will still lock, but the constellation of the received signal will provide a fixed rotation of a multiple of 90° with respect to the constellation of the transmitted signal [41]. A phase ambiguity that may occur at the receiver can be easily corrected using the "Unique Word" technique [26].

2) EXTRACTING THE IMAGE DATA BY USING A DLL-BASED CIRCUIT

The block diagram illustrated in Fig. 11 is used to extract the information from the two received DSSS-CDMA sequences. This block diagram includes a *delay-lock tracking loop* based on the principle illustrated in [15] for *tracking* and an *acquisition* stage based on the SDSS technique [36], [42].

The *delay-lock tracking loop* includes two correlators based on a matched filter, with the schematic illustrated in Fig. 12, which are driven by two local pseudo-noise sequences, "Early" (E) and "Late" (L), which are delayed by one chip. Because the duration of one symbol applied to the correlator's input is equal to $16T_0$ and the duration of one cycle for the PN sequence is $15T_0$, the output of the first multiplier of the correlator illustrated in Fig. 12 is weighted with zero. Each correlator provides a triangular function with two chips wide at the output, as shown in Fig. 13. The resulting correlation function of the DLL has a double-peaked triangular shape, as shown in [15], and a linear region placed on either side of the point in the middle of the distance between the two correlation maxima. Next, the summed correlator outputs are low-pass filtered and used to control the voltage-controlled oscillator (VCO) such that the locally generated PN sequence tracks the incoming code at a point halfway between the maximum and minimum of the composite correlator output [15]. The *acquisition* stage includes a *Correlator*, a comparator (*Comp*) with an absolute value (*Abs*) block at its output, and a simple digital logic, implemented with a counter (*Count*) and a NAND gate.

The output signal provided by the correlator is compared with the threshold level (*Th*). If the threshold is exceeded, the output of the comparator is zero logic, and the output of the NAND gate will be one logic, regardless of the signal applied to its other input, which means that the "CK/Phase generator" block will keep the signal phase provided by the VCO unchanged. If the threshold is not exceeded, the output of the comparator is one logic, which means that the output of the NAND gate depends on the signal applied to its other input. The counter is set to cyclically count 16 clock periods and to provide a synchronization pulse at its output after each counting cycle. Because the clock frequency is 19 kHz, the signal at the output of the counter is represented by a pulse train with a period equal to the period of the symbol data (1/1187.5 s). Thus, the signal from the comparator output will control the "CK/Phase generator" circuit only at time moments that are multiples of the data period. At this time, the output of the NAND gate will be zero logic, which will cause the "CK/Phase generator" block to modify the phase of the VCO signal to achieve the synchronization of the two PN sequences.

After synchronous detection, the two received DSSS-CDMA sequences, $r_{CDMA_I}(t)$ and $r_{CDMA_Q}(t)$, on the two signal paths are multiplied with two pseudo-noise sequences generated locally by the DLL-based circuit to extract the components of the DEQPSK data ($S_I(t)$ and $S_Q(t)$), as shown in Fig. 11.

To obtain the DEQPSK signal corresponding to image j, we multiply the two received DSSS-CDMA signals on both signal paths by the corresponding pseudo-noise binary sequences, locally generated, and delayed by j terms, denoted as $\boldsymbol{p_j}$. Thus, for the time taken to complete one cycle for the PN sequence, the signals at the output of Correlators I and Q in Fig. 11 have constant values and can be written as

$$\begin{cases} r_{Ij} = \boldsymbol{r_{CDMA_I}} \cdot \boldsymbol{p_j^T} \\ r_{Qj} = \boldsymbol{r_{CDMA_Q}} \cdot \boldsymbol{p_j^T}, \end{cases} \quad j = 0, 1, \ldots, n-1 \qquad (27)$$

where $\boldsymbol{r_{CDMA_I}}$ and $\boldsymbol{r_{CDMA_Q}}$ are n-dimensional vectors whose elements represent the values of the signals $r_{CDMA_I}(t)$, $r_{CDMA_Q}(t)$ at times that are multiples of chip duration ($k \cdot T_0$, $k = 1, 2, \ldots$).

By using (21) in (27), the signals obtained at the two correlator outputs are:

$$\begin{cases} r_{Ij} = \left[S_{I0}\boldsymbol{p}_0 + S_{I1}\boldsymbol{p}_1 + \ldots + S_{I(n-1)}\boldsymbol{p}_{(n-1)}\right] \cdot \boldsymbol{p_j^T} \\ r_{Qj} = \left[S_{Q0}\boldsymbol{p}_0 + S_{Q1}\boldsymbol{p}_1 + \ldots + S_{Q(n-1)}\boldsymbol{p}_{(n-1)}\right] \cdot \boldsymbol{p_j^T} \end{cases} \qquad (28)$$

According to the autocorrelation property of PN sequences [32], we have:

$$\boldsymbol{p_i} \cdot \boldsymbol{p_j^T} = \begin{cases} n, & \text{for } i = j \\ -1, & \text{for } i \neq j, \end{cases} \quad i = 0, 1, \ldots, n-1; \quad j = 0, 1, \ldots, n-1 \qquad (29)$$

where $n = 15$ represents the length of the PN sequences used in our radio communication system.

According to (29), considering that the elements of the PN sequences $\boldsymbol{p_j}$ can be "±1" and S_{Ij} and S_{Qj} are equal to "±a" for one cycle of the PN sequence, the signals obtained at the outputs of the two correlators I and Q, corresponding to image j, can be written as

$$\begin{cases} r_{Ij} = S_{I0}\boldsymbol{p}_0\boldsymbol{p_j^T} + S_{I1}\boldsymbol{p}_1\boldsymbol{p_j^T} + \cdots + S_{I(j-1)}\boldsymbol{p}_{(j-1)}\boldsymbol{p_j^T} \\ \qquad + nS_{Ij} + S_{I(j+1)}\boldsymbol{p}_{(j+1)}\boldsymbol{p_j^T} + \cdots + S_{I(n-1)}\boldsymbol{p}_{(n-1)}\boldsymbol{p_j^T} \\ r_{Qj} = S_{Q0}\boldsymbol{p}_0\boldsymbol{p_j^T} + S_{Q1}\boldsymbol{p}_1\boldsymbol{p_j^T} + \cdots + S_{Q(j-1)}\boldsymbol{p}_{(j-1)}\boldsymbol{p_j^T} \\ \qquad + nS_{Qj} + S_{Q(j+1)}\boldsymbol{p}_{(j+1)}\boldsymbol{p_j^T} + \cdots + S_{Q(n-1)}\boldsymbol{p}_{(n-1)}\boldsymbol{p_j^T} \end{cases} \qquad (30)$$

In the following, two cases are analyzed.

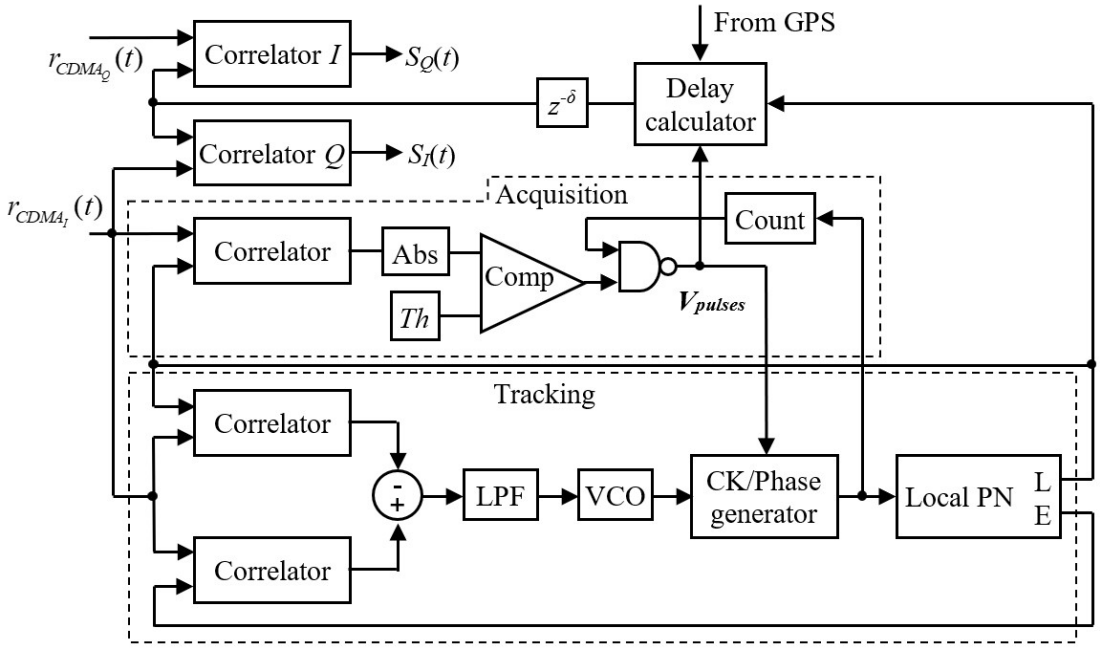

FIGURE 11. Block diagram of the DLL-based demodulator circuit.

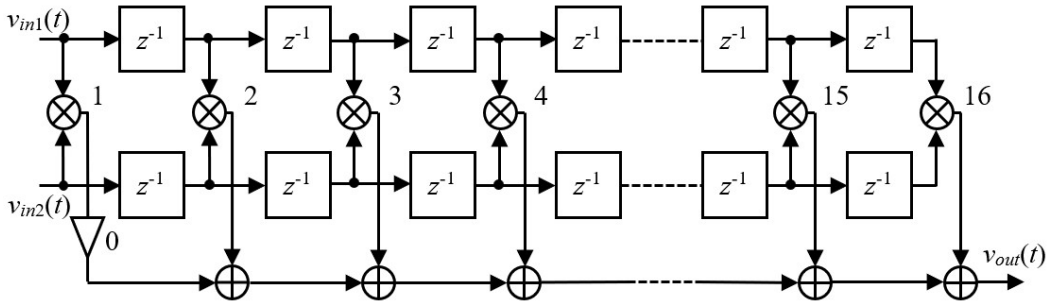

FIGURE 12. Circuit correlator based on matched filter.

Case I. Coordinates of the message point $S_{(I/Q)j} = a > 0$

According to (29) and (30), in this case, the signals obtained at the two correlator outputs are

$$r_{(I/Q)j} = \begin{cases} (2n-1)a, & \text{in the most favorable case} \\ a, & \text{in the worst case} \end{cases} \quad (31)$$

Case II. Coordinates of the message point $S_{(I/Q)j} = -a < 0$

According to (29) and (30), in this case, the signals obtained at the two correlator outputs are

$$r_{(I/Q)j} = \begin{cases} -(2n-1)a, & \text{in the most favorable case} \\ -a, & \text{in the worst case} \end{cases} \quad (32)$$

Because for each case the phase value of the detected signal does not change (as can be seen in (31) and (32)), the detection of the message points is still possible, and the DEQPSK signal $s_{DEQPSK_j} = S_{Ij} + j \cdot S_{Qj}$ is obtained. This signal is then demodulated to extract the transmitted j image.

In Fig. 14, the constellations of the received multi-level DSSS-CDMA signals (scaled for $a = 1$) for different numbers of images transmitted simultaneously on an AWGN communication channel are presented. According to these simulation results, the constellations of the received signal are similar to those of M-QAM signals, whose message points are pseudo-randomly generated. In Fig. 15, the constellations of the DEQPSK signal, corresponding to one received image recovered by the DLL-based circuit for different numbers of images transmitted simultaneously are presented.

The *Correlator*, *Abs* and *Comparator* blocks from the *Acquisition* stage illustrated in Fig. 11 are used to determine whether synchronization of the two PN sequences has been achieved. According to the previous discussion, and equations (31)-(32), for a number of $n = 15$ images transmitted simultaneously, the signal provided by the *Correlator* and *Abs*

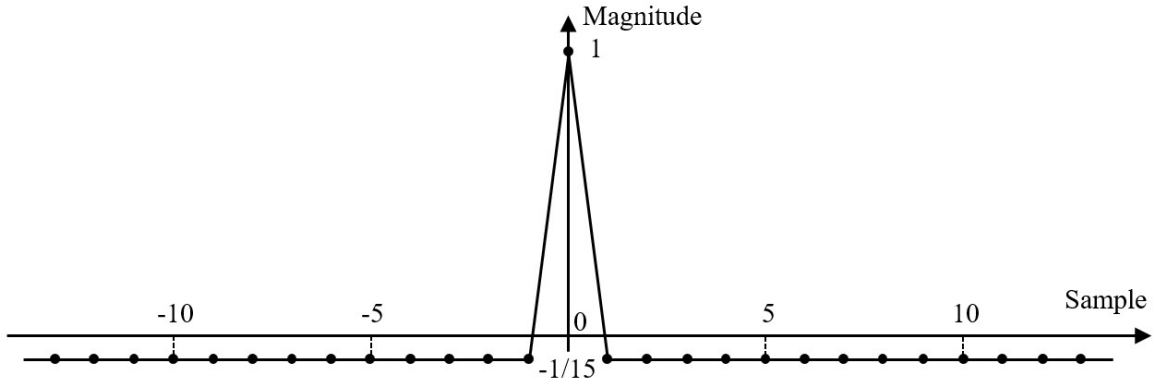

FIGURE 13. Autocorrelation function of a PN sequence of length equal to 15.

blocks from the *Acquisition* stage in Fig. 11 varies between a *maximum* and a *minimum* value, given by:

$$\begin{cases} |V_{max}| = (2n-1)a = 29a \\ |V_{min}| = a, \end{cases} \quad a > 0. \tag{33}$$

Thus, for a number of q images transmitted simultaneously, the maximum and minimum values provided by the *Correlator* and *Abs* blocks from the *Acquisition* stage in Fig. 11 can be written as:

$$\begin{cases} |V_{\boldsymbol{max}}| = [n + (q-1)]\, a \\ |V_{min}| = [n - (q-1)]\, a, \end{cases} \quad q = 1, 2, \ldots, n \tag{34}$$

The minimum value obtained at the correlator output, V_{min}, represents the threshold (Th) used in the block diagram in Fig. 11 to detect whether synchronization of the two pseudo-noise sequences was performed.

Thus, for $n = 15$, the threshold value (Th), depending on q number of images transmitted simultaneously ($q \leq 15$), is

$$Th = [15 - (q-1)]\, a, \quad q = 1, 2, \ldots, 15 \tag{35}$$

Thus, if the correlator output varies between V_{min} and V_{max}, the two pseudo-noise sequences are synchronized. For values lower than V_{min}, the synchronization of the two pseudo-noise sequences is not achieved. This can be observed in the constellation diagrams of the detected DEQPSK signal, as shown in Fig. 15.

According to (35), the more images we send simultaneously (increasing the noise on the communication channel), the lower is the threshold value used as a synchronization indicator for the two pseudo-noise sequences. The minimum value of the threshold ($Th = a$) was achieved when 15 images were simultaneously transmitted.

If 15 images are transmitted simultaneously and the DLL is locked, the minimum value that can be obtained at the output of the *Correlator* and *Abs* blocks from the *Acquisition* stage in Fig. 11 in ideal conditions cannot be less than the threshold value used in this case, which is equal to "a". Due to the noise, the value obtained at the output of the *Correlator* and *Abs* blocks in Fig. 11 could be less than the threshold value, which will cause a phase change in the locally generated PN sequence, which will lead to the desynchronization of the loop. Therefore, the maximum acceptable value of the noise power must consider the Euclidean distance between two adjacent points in the signal constellation, which is equal to $2a$. The noise power can be written as

$$P_{noise} < 2a^2 \tag{36}$$

The number of pulses (n_{pulses}) produced by the V_{pulses} signal in Fig. 11, which generates the phase change of the locally generated PN sequence, provides information regarding the image on which the DLL was locked after the end of the acquisition regime. Thus, the number j of the image on which the loop was locked can be determined by using the modulo (mod) operation, as follows:

$$j = n_{pulses} \bmod 15 \tag{37}$$

This information is then processed by a digital logic ("Delay calculator" in Fig. 11), which establishes the necessary delay δ of the PN sequence to generate the image corresponding to the vehicle location at the output. After the DLL circuit was locked, the circuit that generates the phase change in the "CK / Phase generator" block based on V_{pulses} signal can be deactivated, in order to avoid accidental phase changes, after the synchronization of the two PN sequences. During this period, the loop is synchronized by the tracking mechanism, which is functional at all times.

In the case of a practical implementation of the system, to avoid any synchronization errors, the image identification number could be included in the header of each transmitted image, and will be received after synchronization. Then the digital logic will calculate the necessary delay δ for receiving the image corresponding to the respective location.

III. SIMULATION AND EXPERIMENTAL RESULTS

The proposed radio communication system was tested by simulations performed using the MATLAB/Simulink software and by using an experimental setup including two USRP devices [43] configured as a transmitter and receiver.

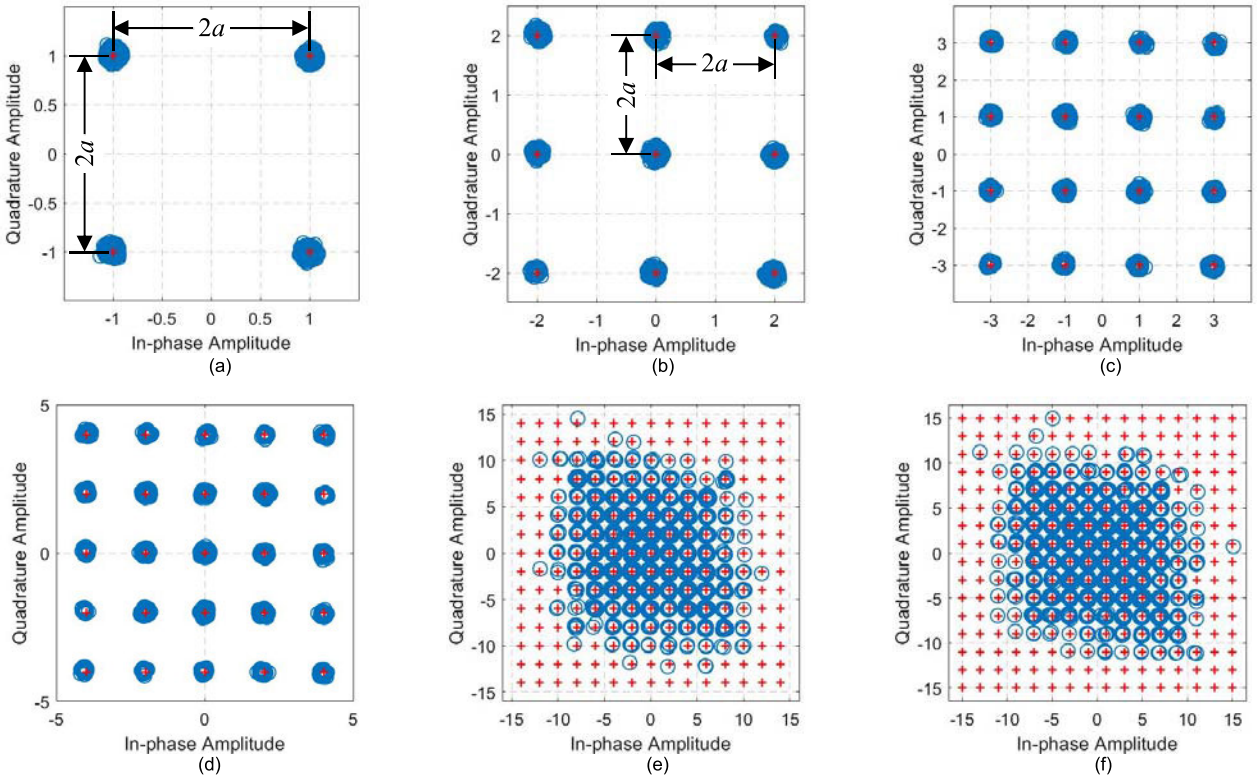

FIGURE 14. Constellations of the received multi-level DSSS-CDMA signals (scaled for $a = 1$) for different number of images transmitted simultaneously on an AWGN channel: (a) 1 image ($M = 4$); (b) 2 images ($M = 9$); (c) 3 images ($M = 16$); (d) 4 images ($M = 25$); (e) 14 images ($M = 225$); (f) 15 images ($M = 256$).

TABLE 2. Parameters of the DSSS-CDMA transmission.

Data rate of each image (f_b) [bit/s]	Symbol rate of each DEQPSK image (f_s) [symbol/s]	Spreading factor (SF)	PN chip rate (f_{ch}) [kHz]	Subcarrier freq. (f_c) [kHz]	Sampling rate [kHz]
2375	1187.5	16	19	76	228

A. SIMULATION RESULTS

The simulation setup includes a transmitter, implemented based on the block diagram illustrated in Fig. 5, and a receiver, implemented using the circuit presented in Fig. 8. For the simulation setup, the baseband FM signal was generated (the carrier frequency was set to 0 Hz), and an AWGN communication channel was used.

All transmission scenarios, including 1, 2, 3, . . . , 15 images transmitted simultaneously using the DSSS-CDMA technique in a standard FM transmission, were tested by simulation. In our tests, 15 images were used, representing different traffic events, as illustrated in Fig. 2.

Table 2 lists the parameters of the DSSS-CDMA transmission used in the simulations. The standard parameters of FM transmissions in terms of the frequency deviation ($\Delta f = 75$ kHz) and weights of the different spectral components [26] were used in the simulation.

In the following, the simulation results for the case when 15 images are transmitted simultaneously and for a signal-to-noise ratio of the DSSS-CDMA data onto a 76 kHz subcarrier (SNR_{CDMA}) equal to 22 dB are presented.

In Fig. 16, the following frequency spectra are illustrated: the spectrum of the transmitted baseband FM signal (Fig. 16 (a)); the spectrum of the transmitted and received customized baseband signal, which includes the stereo MPX component and the DSSS-CDMA data onto a subcarrier of 76 kHz (Figs. 16 (b) and (c), respectively); the spectrum of the received stereo MPX component obtained at the output of the LPF in Fig. 8 is presented in Fig. 16 (d); the spectrum of the received DSSS-CDMA data onto a 76 kHz subcarrier obtained at the output of the BPF in Fig. 8 is presented in Fig. 16 (e); the spectrum of the received audio stereo signal is shown in Fig. 16 (f). As presented in Figs. 16 (b) and (c), the spectrum of the transmitted and received customized baseband signal include the spectrum of the MPX signal, corresponding to standard FM transmission (between DC – 53 kHz), and the spectrum of the DSSS-CDMA data onto a 76 kHz subcarrier, which occupies a frequency bandwidth of 38 kHz in a range between 53 and 99 kHz. Considering the trade-off between the date rate and BER required for optimal image transmission, using the DSSS-CDMA technique, it is possible to transmit a maximum of 15 images in a frequency bandwidth between 53 and 99 kHz at the same time with the standard FM broadcasting.

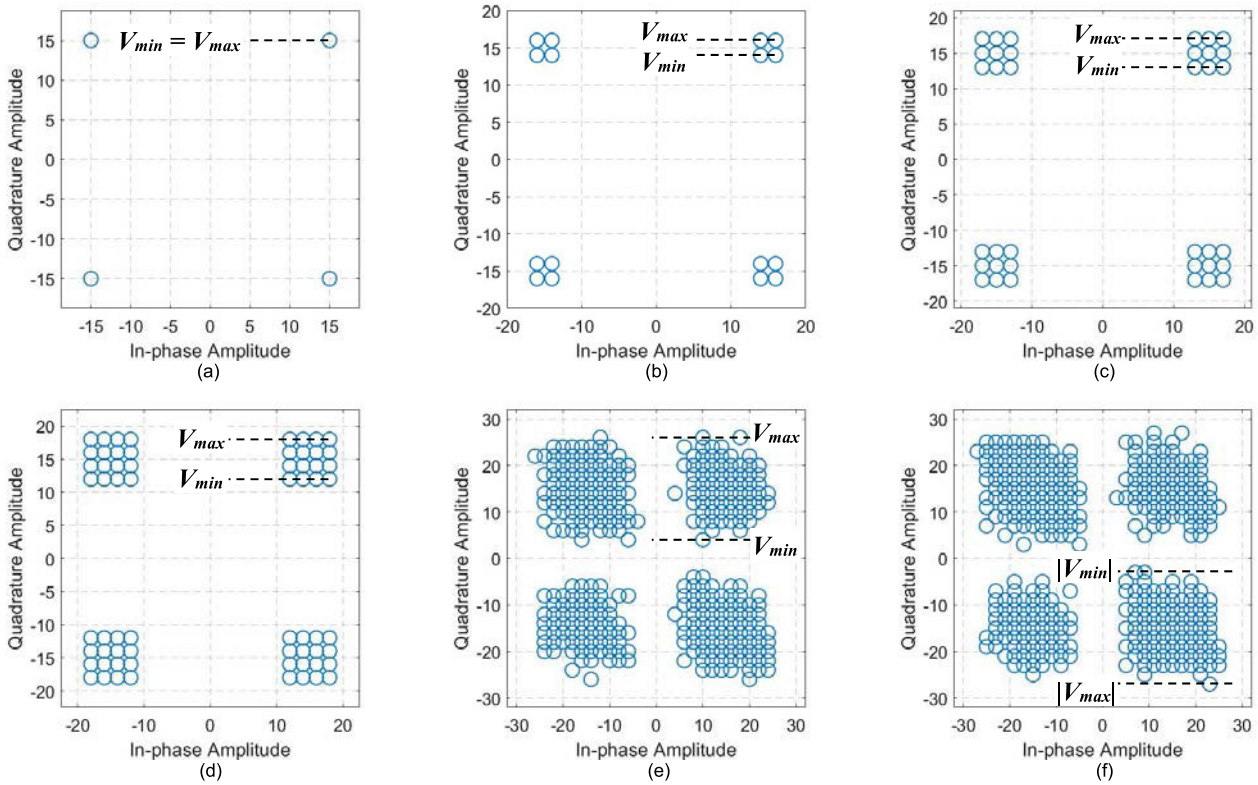

FIGURE 15. Constellations of the received DEQPSK signals (scaled for $a = 1$) provided by the DLL-based circuit for different number of images transmitted simultaneously on an AWGN channel: (a) 1 image; (b) 2 images; (c) 3 images; (d) 4 images; (e) 14 images; (f) 15 images.

For the same radio communication scenario, in Fig. 17, the following constellations (scaled for $a = 1$) are presented: the constellation of the DSSS-CDMA signal corresponding to one transmitted image (Fig. 17 (a)), constellation of the transmitted multi-level DSSS-CDMA signal (Fig. 17 (b)), constellation of the received multi-level DSSS-CDMA signal provided by the Costas loop (Fig. 17 (c)), and constellation of the received DEQPSK signal provided by the DLL-based circuit corresponding to one received image (Fig. 17 (d)).

In Fig. 18, we present some received images for the scenario when all set of 15 images are simultaneously transmitted for different values for the signal-to-noise ratio of the DSSS-CDMA data onto a 76 kHz subcarrier.

In order to test the performance of the DSSS-CDMA communication system, regarding its capability to simultaneously transmit as accurately as possible different number of images, the BER value depending on signal-to-noise ratio of the data signal is calculated. To increase the accuracy of the BER estimation, the DLL-based demodulator circuit was disabled and the clock signal used for the local generation of the PN sequence was extracted from the pilot tone of the received MPX stereo signal. Under ideal conditions (considering an AWGN communication channel), this is possible because the chip frequency of the CDMA signal is chosen to be equal to 19 kHz, which is the frequency of the pilot tone.

In Fig. 19, the BER depending on the signal-to-noise ratio of the received multi-level CDMA signals onto a 76 kHz subcarrier for different numbers of images transmitted simultaneously is presented. The BER vs. *SNR* curves illustrated in Fig. 19 were drawn by calculating the *SNR* value obtained from the simulation using the software spectrum analyzer (set to display a two-sided spectrum) from the MATLAB/Simulink program.

The BER plots were obtained considering 100660 bits transmitted on the communication channel, representing an image with a resolution of 100 × 100 pixels. The BER accuracy depends on the number of bits transmitted, and for our simulations, it was limited to $9.934 \cdot 10^{-6}$ (1/100660).

Due to the spectral spreading of the DSSS-CDMA signal, its signal-to-noise ratio can be written as

$$SNR_{CDMA}|_{\text{dB}} = SNR_I|_{\text{dB}} - 10 \log SF \tag{38}$$

where $SF = 16$ is the spreading factor of the DSSS-CDMA sequence and SNR_I is the signal-to-noise ratio of the non-spread input signal. In this way, the low *SNR* values (even lower than 0 dB for fewer than four images transmitted simultaneously) illustrated in Fig. 19 can be explained.

According to these simulation results, for the scenario in which all 15 images are transmitted simultaneously, the minimum value of the signal-to-noise ratio of the received multi-level CDMA signals onto a 76 kHz subcarrier for

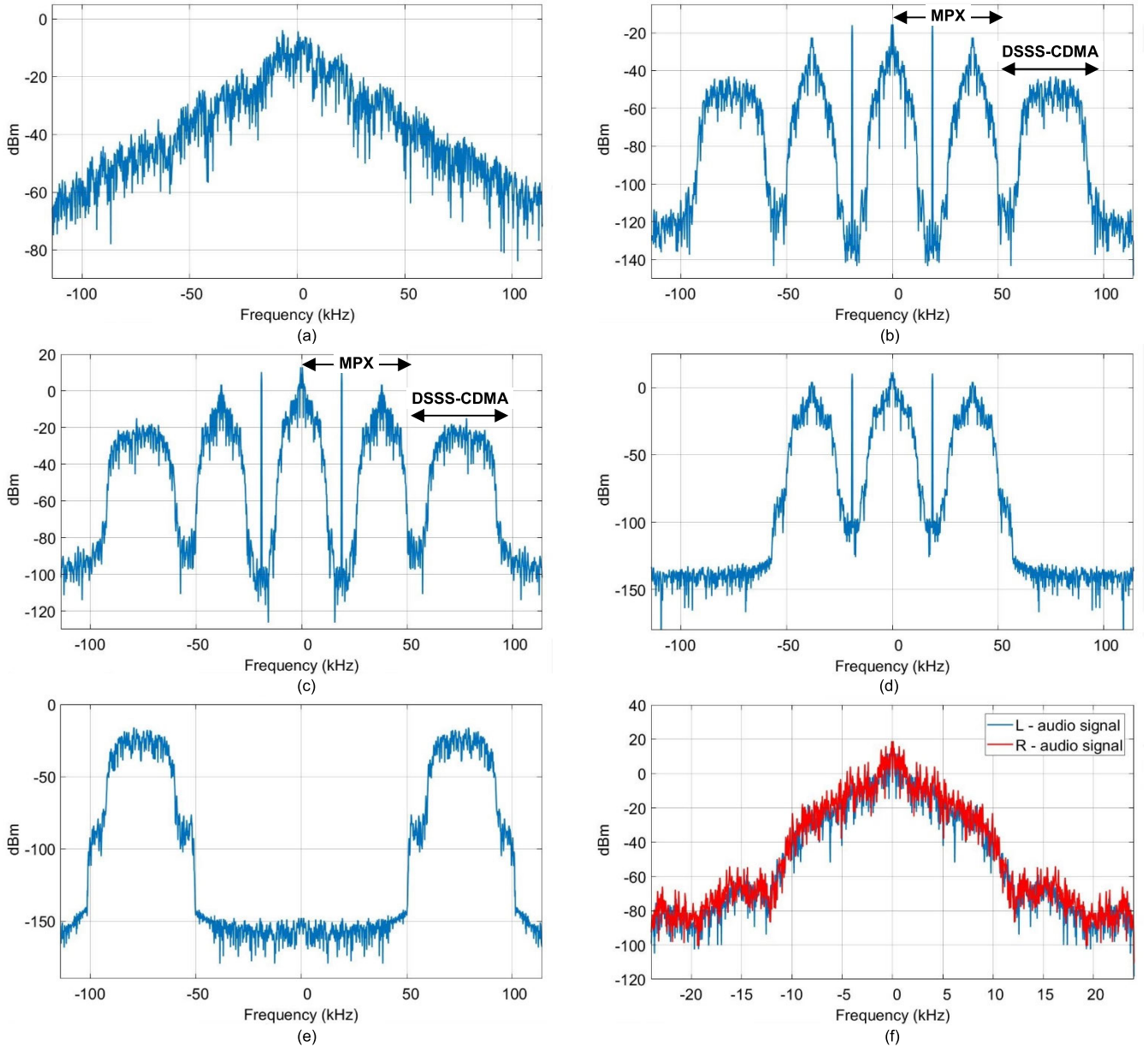

FIGURE 16. Simultaneous transmission of 15 images with DSSS-CDMA modulation within a stereo FM transmission by using a $SNR_{CDMA} = 22$ dB: (a) Spectrum of the transmitted baseband FM signal; (b) Spectrum of the transmitted customized baseband signal; (c) Spectrum of the received customized baseband signal; (d) Spectrum of the received stereo MPX signal; (e) Spectrum of the received DSSS-CDMA signal; (f) Spectrum of the received audio stereo signal.

which an image is received with the highest possible quality (BER $= 1.987 \cdot 10^{-5}$) is $SNR_{CDMA} = 22$ dB.

In Fig. 20, the BER depending on the signal-to-noise ratio of the received DEQPSK images (SNR_{DEQPSK}) for different numbers of images transmitted simultaneously is shown. The constellations of these signals are shown in Fig. 15.

Fig. 21 illustrates the variation range of the signal-to-noise ratio for the received DEQPSK signals, corresponding to one received image, depending on the number of images transmitted simultaneously for which their reception is performed with the highest quality (red curve, for which BER $= 1.987 \cdot 10^{-5}$) and with the lowest quality (blue curve, for which BER varies between $1.17 \cdot 10^{-1}$ and $1.54 \cdot 10^{-1}$).

In Table 3, the BER depending on the signal-to-noise ratio of the received DEQPSK images (required to obtain high- and low-quality images) for different numbers of images transmitted simultaneously is illustrated.

According to these simulation results, for the scenario in which sets of one to nine images are transmitted simultaneously, the minimum value of SNR_{DEQPSK} for which an image is received with the highest possible quality (red curve in

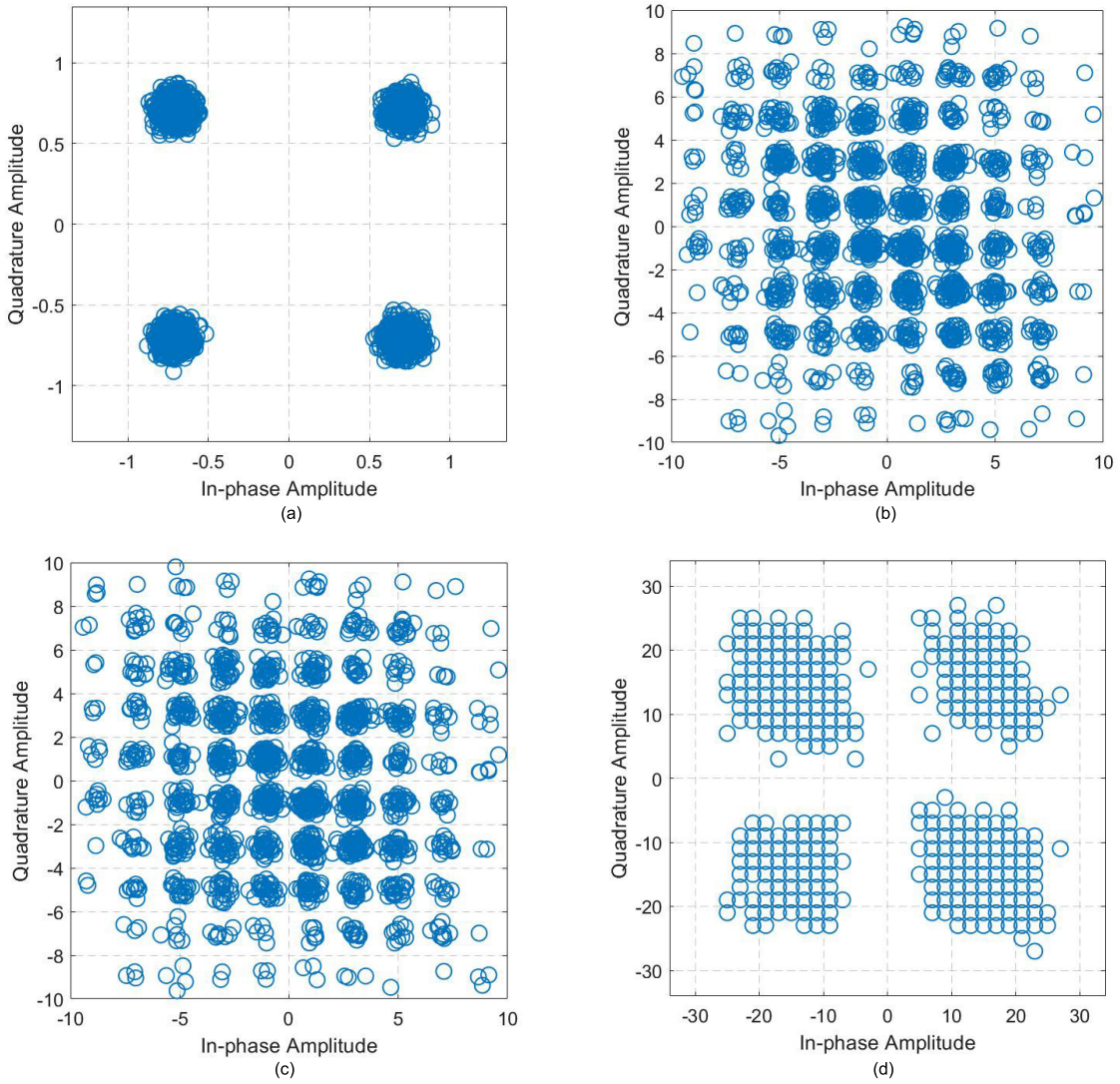

FIGURE 17. (a) Constellation of the DSSS-CDMA signal corresponding to one transmitted image; (b) Constellation of the multi-level DSSS-CDMA signal corresponding to all 15 images transmitted simultaneously; (c) Constellation of the received multi-level DSSS-CDMA signal corresponding to all 15 images transmitted simultaneously; (d) Constellation of the received DEQPSK signal corresponding to one received image; (SNR_{CDMA} = 22 dB).

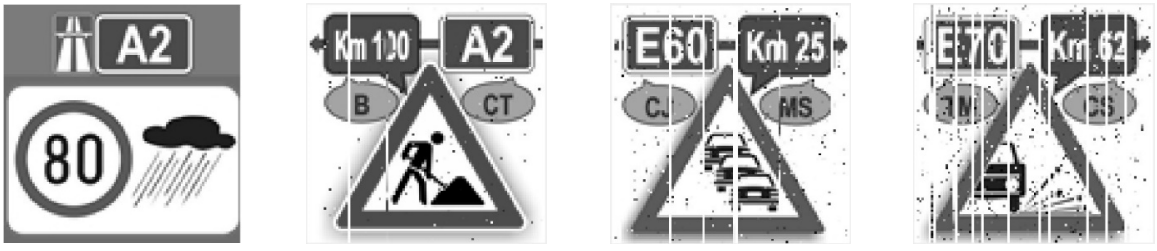

(a) (b) (c) (d)

FIGURE 18. Some received images for the situation when all 15 images are transmitted simultaneously with different value of the SNR_{CDMA}: (a) SNR_{CDMA} = 22 dB; BER = 0; b) SNR_{CDMA} = 13 dB; BER = 0.004838; c) SNR_{CDMA} = 11 dB; BER = 0.01315; d) SNR_{CDMA} = 9 dB; BER = 0.02774.

Fig. 21) is approximately constant, ranging from 14 to 16 dB. For sets of 10 – 15 images transmitted simultaneously, the value of SNR_{DEQPSK} increased significantly, being between 18 and 32 dB.

On the other hand, the minimum SNR_{DEQPSK} value of the received DEQPSK signals for which image reception is still possible, but at the lowest quality (blue curve in Fig. 21) is between 3.4 and 4.3 dB.

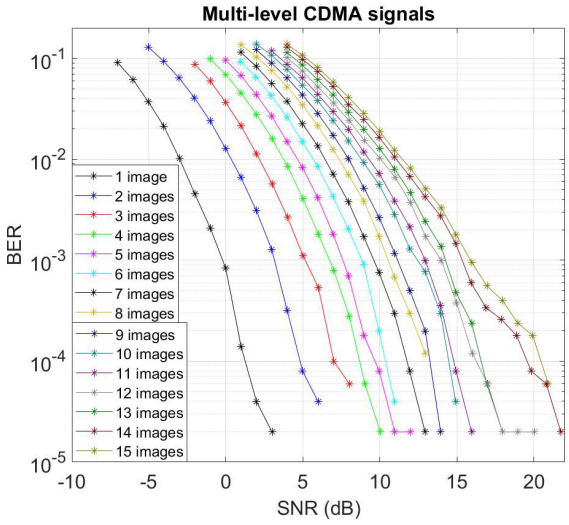

FIGURE 19. BER depending on the *SNR* of the received multi-level CDMA signals onto a 76 kHz subcarrier for different number of images transmitted simultaneously.

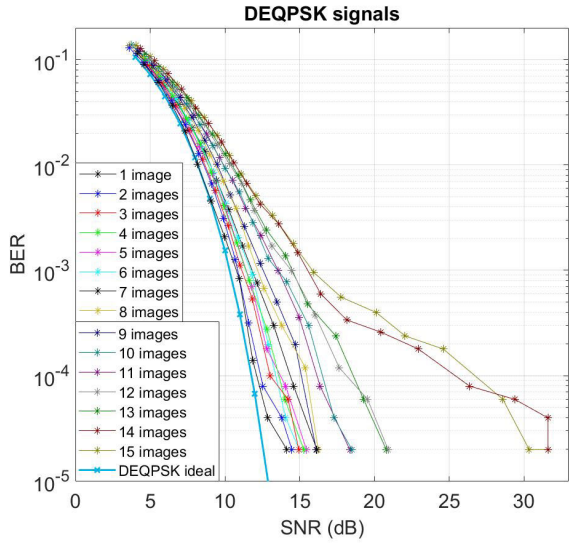

FIGURE 20. BER depending on the *SNR* of the received DEQPSK images for different number of images transmitted simultaneously together with the ideal BER curve of the DEQPSK signal.

Next, the performance of the entire radio communication system, including the DLL-based demodulator circuit illustrated in Fig. 8, is tested.

According to the simulation results, for the scenario in which all set of 15 images are transmitted simultaneously and the DLL-based circuit operates properly, the minimum value of the signal-to-noise ratio of the received multi-level DSSS-CDMA signals onto a 76 kHz subcarrier for which an image is received with the lowest BER (BER $= 1.987 \cdot 10^{-5}$) is equal to 22 dB, as in the previous case.

For the same transmission scenario, the minimum signal-to-noise ratio of the received DEQPSK signal for which an image is received with the lowest BER is equal to 32 dB.

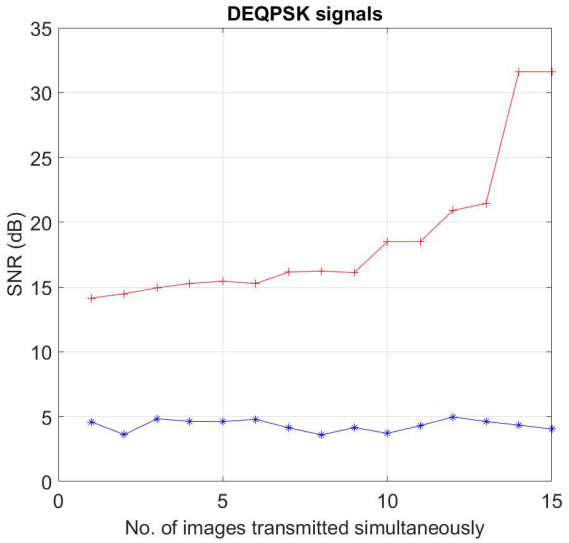

FIGURE 21. Variation range of the *SNR* for the received DEQPSK signals depending on number of images transmitted simultaneously in which their reception is performed with high-quality (red curve, for which BER $= 1.987 \cdot 10^{-5}$) and with low-quality (blue curve, for which BER $= [1.17 \cdot 10^{-1}; 1.54 \cdot 10^{-1}]$.

TABLE 3. Performance of the proposed DSSS-CDMA transmission in terms of BER depending on SNR_{DEQPSK} required to obtain high- and low-quality images.

Number of images transmitted simultaneously (n)	High-quality image		Low-quality image	
	SNR_{DEQPSK} [dB]	BER	SNR_{DEQPSK} [dB]	BER
1	14.1471	$1.987 \cdot 10^{-5}$	3.8249	$1.182 \cdot 10^{-1}$
5	15.4531	$1.987 \cdot 10^{-5}$	4.0685	$1.17 \cdot 10^{-1}$
9	16.1133	$1.987 \cdot 10^{-5}$	3.7604	$1.334 \cdot 10^{-1}$
10	18.4940	$1.987 \cdot 10^{-5}$	3.4315	$1.496 \cdot 10^{-1}$
12	20.9197	$1.987 \cdot 10^{-5}$	4.2966	$1.237 \cdot 10^{-1}$
15	31.6051	$1.987 \cdot 10^{-5}$	3.5971	$1.54 \cdot 10^{-1}$

To test the performance of the Costas loop and of the DLL-based circuit by simulation, different frequency offsets (Δf) between -100 Hz and 100 Hz, around a pilot tone of 19 kHz, were applied at the transmitter circuit.

The optimal operation of the Costas loop depends on the value of the loop step k_0 and gain A applied at the output of the multipliers from Fig. 9, which can be established by means of an automatic gain control (AGC) circuit. The AGC circuit was not implemented during this stage of the study.

The operation of the Costas loop is illustrated in Fig. 22 (a), which presents the phase correction provided by the loop for a $SNR_{CDMA} = 22$ dB of the digital signal and a frequency offset $\Delta f = 100$ Hz of the 19 kHz pilot tone. This frequency offset represents a frequency deviation of 400 Hz for the 76 kHz subcarrier. The capture range of the Costas loop is limited by the frequency bandwidth of the peak filter implemented to select the pilot tone from the Stereo FM Demultiplexer stage, which is equal to 200 Hz, around the 19 kHz frequency. For the same parameters of the simulation setup, the error signal

provided by the DLL-based circuit (signal obtained at the LPF output from the *Tracking* stage of the DLL-based circuit from Fig. 11) is illustrated in Fig. 22 (b).

Considering a number of 100660 bits transmitted on the communication channel, for frequency offsets $\Delta f = -100$ Hz and $\Delta f = 100$ Hz, a BER equal to $7.948 \cdot 10^{-5}$ (which means 8 error bits) and $1.987 \cdot 10^{-5}$ (which means 2 error bits) have been obtained, respectively.

B. EXPERIMENTAL RESULTS

As shown in Fig. 23, the experimental setup includes two USRPs of type N210 configured as transmitter and receiver. The proposed radio communication system was tested under laboratory conditions, and the two USRPs were placed at a distance of approximately 3 m between them.

The architecture of USRP N210 includes a Xilinx Spartan 3A-DSP 3400 FPGA, 100 MS/s dual ADC, 400 MS/s dual DAC and Gigabit Ethernet connectivity to stream data to and from host processors. The device operates from DC to 6 GHz. The two USRP N210 used for the experimental setup included a WBX USRP daughterboard, which is a wide bandwidth transceiver that provides up to 100 mW of output power and a noise figure of 5 dB [43]. The WBX provides a bandwidth capability of 40 MHz and can be used for applications requiring access to a number of different bands within its range – 50 MHz to 2.2 GHz [43].

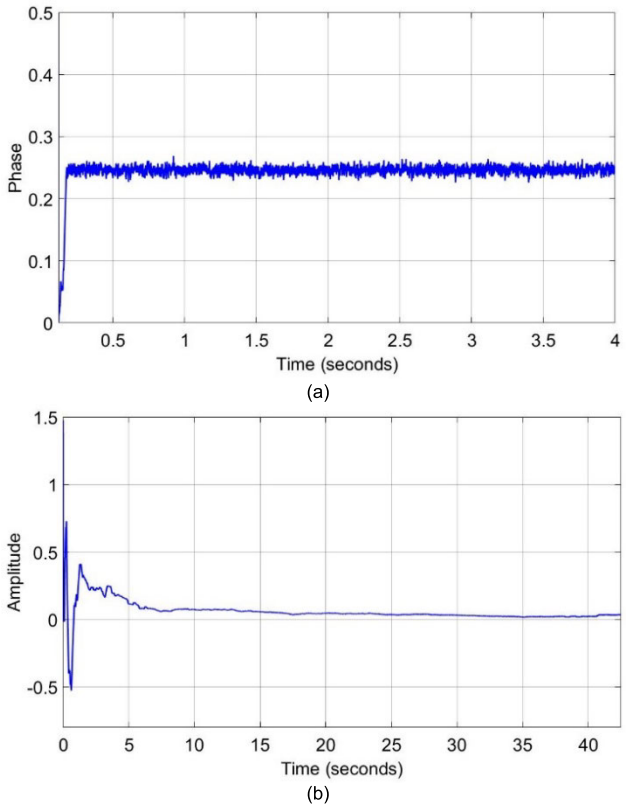

FIGURE 22. (a) Phase correction provided by the Costas loop for a frequency offset $\Delta f = 100$ Hz of the 19 kHz pilot tone; (b) Error signal provided by the DLL-based circuit.

In order to perform the simulations in MATLAB/Simulink by using USRP N210 devices, the Communications System Toolbox Support Package for USRP Radio has been installed.

The two USRP N210 use a monopole-type telescopic antenna, with a frequency range between 25 Hz and 1900 MHz and a length in the range of 70 – 340 mm.

The customized baseband signal, used by the USRP device configured as a transmitter, is generated based on the circuit illustrated in Fig. 5. The second USRP device, configured as a receiver, provides the received baseband FM signal to the software program (MATLAB/Simulink), which is demodulated with the software-defined radio receiver illustrated in Fig. 8.

The proposed radio communication system was tested for different operating scenarios, in which 1, 3, 5, 9, 11, and 15 images were transmitted simultaneously. All transmissions were performed under identical conditions, using the same transmission power level for the RF signal. The RF frequency was set at 109 MHz. The spectrum of the received customized baseband signal is illustrated in Fig. 24. This signal includes the stereo MPX signal and the DSSS-CDMA data onto a 76 kHz subcarrier for the scenario in which all 15 images are transmitted simultaneously.

In Table 4 the experimental results are presented.

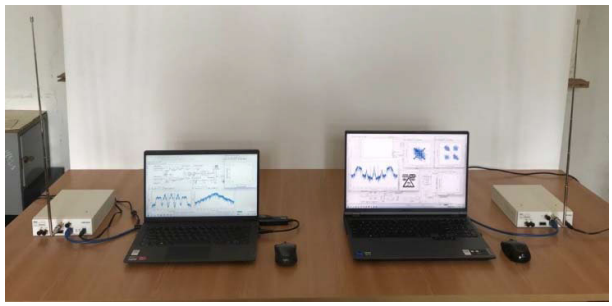

FIGURE 23. Experimental setup including two N210 USRPs configured as transmitter (left) and as receiver (right).

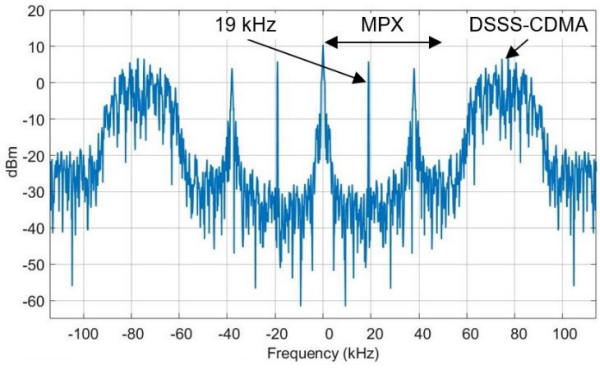

FIGURE 24. Spectrum of the received customized baseband signal for the scenario when all 15 images are simultaneously transmitted by using a DSSS-CDMA modulation onto a 76 kHz subcarrier.

The signal-to-noise ratio of the received multi-level DSSS-CDMA signal was measured using a software spectrum analyzer from MATLAB/Simulink.

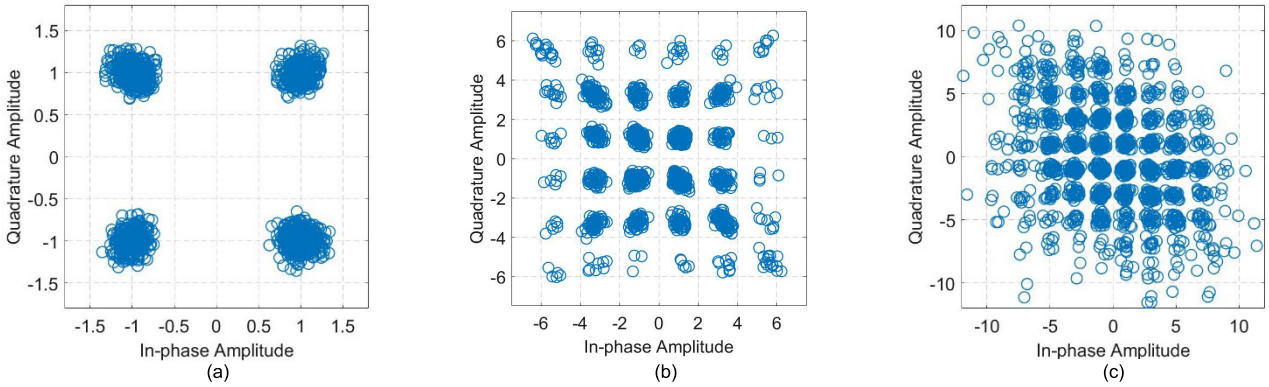

FIGURE 25. Constellations of the received multi-level DSSS-CDMA signals (scaled for $a = 1$) for different number of images transmitted simultaneously: (a) 1 image; (b) 5 images; (c) 15 images.

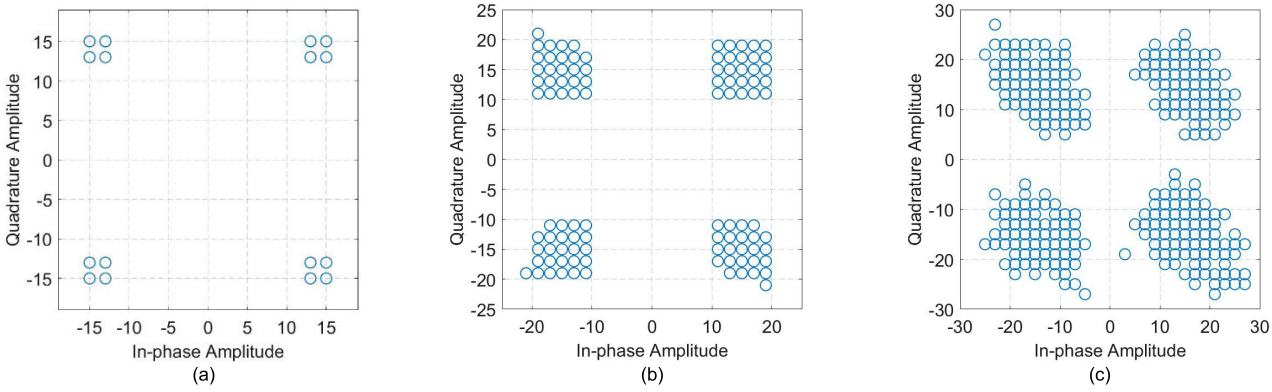

FIGURE 26. Constellations of the received DEQPSK signals (scaled for $a = 1$) provided by the DLL-based circuit for different number of images transmitted simultaneously: (a) 1 image; (b) 5 images; (c) 15 images.

TABLE 4. Experimental results.

Number of images transmitted simulta-neously (n)	Transmission power of the RF signal [dBm] (approx.)	Received power of the RF signal [dBm]	SNR_{CDMA} [dB]	BER
1	-10	-4.257	18.64	0
3	-10	-5.428	20.95	0
5	-10	-4.691	23.29	0
15	-10	-2.741	21.88	$11.92 \cdot 10^{-5}$

For the case in which all 15 images are transmitted simultaneously, the signal-to-noise ratio of the received multi-level DSSS-CDMA signal onto a 76 kHz subcarrier that was measured was approximately 21.88 dB and the number of error bits was 12 from a total of 100660 transmitted bits (BER $= 11.92 \cdot 10^{-5}$). For cases in which up to five images were transmitted, there were no error bits. These measurements agree with the results obtained by simulations, as illustrated in Fig. 19, and are confirmed by the theoretical results. Despite the signal-to-noise ratio variations illustrated in Table 4, due to imperfections in the propagation channel under laboratory conditions, the obtained values ensure the optimal transmission of all sets of images.

Fig. 25 presents the constellations of the received multi-level DSSS-CDMA signals (scaled for $a = 1$) provided by the Costas loop for different numbers of images transmitted simultaneously. The results were obtained using the experimental setup shown in Fig. 23. In Fig. 26, the constellations of the received DEQPSK signals (scaled for $a = 1$), corresponding to one received image, provided by the DLL-based circuit, for different numbers of images transmitted simultaneously are shown.

Depending on the communication channel noise, to provide the required *SNR* for the data signal, it may be necessary to increase the power level of the DSSS-CDMA signal spectrum onto a 76 kHz subcarrier with the impairment of the other spectral components. In extreme situations, to avoid exceeding the total modulation level allowed in standard FM transmissions (105.2%), stereo FM transmission can be replaced by mono FM transmission.

The experimental results illustrated in Figs. 24 - 26 confirm the theoretical results and the functionality of the proposed radio communication system.

IV. CONCLUSION

In this paper, a new drivers' warning application for different traffic events using personalized pictograms included

in radio FM broadcasting have been presented. The proposed application is based on a radio communication system capable of simultaneously transmitting a maximum of 15 images representing different warning messages sent by road authorities for drivers located in different geographical areas together with the standard FM signal. Each warning pictogram is transmitted with a data rate of 2375 bit/s, but the proposed system is able to provide a maximum data rate of 35.625 kbit/s when all 15 images are transmitted simultaneously using the DSSS-CDMA modulation technique. The system is implemented using software-defined radio technology, and as a result, it is relatively cheap, flexible, and easy to use by drivers, and is based on existing and widespread radio FM infrastructure.

The proposed application uses a novel implementation of a software-defined radio receiver, which can be easily installed on a car tablet, being able to receive the data notification together with the standard FM radio transmission. To receive the data signal, the proposed radio receiver uses a modified Costas-type synchronization loop on the 76 kHz subcarrier, as well as a DLL-based circuit to ensure time synchronization between the PN sequence of the transmitter with that generated at the receiver stage.

The proposed radio communication system was tested by simulations performed in MATLAB/Simulink, as well as in laboratory conditions, using an experimental setup that included two USRP-type devices configured as a transmitter and a receiver.

According to the simulation results, confirmed by the experimental tests, for the maximum quality reception of each image (BER $\leq 1.987 \cdot 10^{-5}$) from a set of 15 images transmitted simultaneously, the proposed system must ensure a signal-to-noise ratio of the received multi-level CDMA signals higher than 22 dB. This means that the signal-to-noise ratio is higher than 32 dB for each received DEQPSK image.

Unlike other driver warning systems, the proposed radio communication system uses the DSSS-CDMA technique, which allows a significant increase in the amount of data transmitted over the FM radio and increases the robustness of the data signal to natural interference, noise, and jamming.

In future work, the influence of multipath propagation and mobility aspects impacting the proposed radio communication system will be studied.

REFERENCES

[1] The Top 10 Causes of Death. (Dec. 2020). *World Health Organization*. Accessed: Jan. 7, 2023. [Online]. Available: https://www.who.int/news-room/fact-sheets/detail/the-top-10-causes-of-death

[2] Rob Decae (SWOV). *Annual Statistical Report on Road Safety in the EU 2021*. Version 2.0 (Apr. 2022). European Road Safety Observatory. Accessed: Jan. 7, 2023. [Online]. Available: https://road-safety.transport.ec.europa.eu/statistics-and-analysis/data-and-analysis/annual-statistical-report_en

[3] *Rapport de Situation Sur la Sécurité Routière Dans le Monde 2018. Organisation Mondiale de la Santé*. Accessed: Jan. 7, 2023 [Online]. Available: https://apps.who.int/iris/bitstream/handle/10665/277372/WHO-NMH-NVI-18.20-fre.pdf?ua=1

[4] (Mar. 28, 2022). *Road Safety in the EU: Fatalities in 2021 Remain Well Below Pre-Pandemic Level*. Directorate-General for Mobility and Transport. Accessed: Jan. 7, 2023. [Online]. Available: https://road-safety.transport.ec.europa.eu/news-events/news/road-safety-eu-fatalities-2021-remain-well-below-pre-pandemic-level-2022-03-28_en

[5] D. Babić, M. Fiolić, D. Babić, and T. Gates, "Road markings and their impact on driver behaviour and road safety: A systematic review of current findings," *J. Adv. Transp.*, vol. 2020, pp. 1–19, Aug. 2020, doi: 10.1155/2020/7843743.

[6] J. Theeuwes, "Self-explaining roads: Subjective categorisation of road environments," *Vis. Veh.*, vol. 6, pp. 279–287, Jan. 1998.

[7] F. Jiménez, J. E. Naranjo, J. J. Anaya, F. García, A. Ponz, and J. M. Armingol, "Advanced driver assistance system for road environments to improve safety and efficiency," *Transp. Res. Proc.*, vol. 14, pp. 2245–2254, Jan. 2016, doi: 10.1016/j.trpro.2016.05.240.

[8] (Jun. 19, 2019). *EU Road Safety Policy Framework 2021-2030 Next Steps Towards, Vision Zero*. European Commission. Accessed: Jan. 7, 2023. [Online]. Available: https://transport.ec.europa.eu/system/files/2021-10/SWD2190283.pdf

[9] R. G. Bozomitu, F. D. Hutu, and N. D. P. Ferreira, "Drivers' warning application through image notifications on the FM radio broadcasting infrastructure," *IEEE Access*, vol. 9, pp. 13553–13572, 2021.

[10] (Dec. 5, 2017). *An Assessment of LTE-V2X (PC5) and 802.11p Direct Communications Technologies for Improved Road Safety in the EU*. 5G Automot. Assoc. Accessed: Jan. 7, 2023. [Online]. Available: http://5gaa.org/wp-content/uploads/2017/12/5GAA-Road-safety-FINAL2017-12-05.pdf

[11] D. Torrieri, *Principles of Spread-Spectrum Communication Systems*, vol. 1. Berlin, Germany: Springer, 2005.

[12] M. Rice, *Digital Communications: A Discrete-Time Approach*. London, U.K.: Pearson, 2009.

[13] J. S. Lee and L. E. Miller, *CDMA Systems Engineering Handbook*. Norwood, MA, USA: Artech House, 1998.

[14] A. J. Viterbi, *CDMA: Principles of Spread Spectrum Communication*. Boston, MA, USA: Addison Wesley, 1995.

[15] R. C. Dixon, *Spread Spectrum Systems*, 7nd ed. Hoboken, NJ, USA: Wiley, 1984.

[16] M. A. Abu-Rgheff, *Introduction to CDMA Wireless Communications*. New York, NY, USA: Academic, 2007.

[17] A. Goldsmith, *Wireless Communications*. Cambridge, U.K.: Cambridge Univ. Press, 2005.

[18] K. K. Wong and T. O'Farrell, "Spread spectrum techniques for indoor wireless IR communications," *IEEE Wireless Commun.*, vol. 10, no. 2, pp. 54–63, Apr. 2003.

[19] D. R. Taylor, J. Walker, and B. Strunz, "Direct sequence spread spectrum experiments using GNU radio companion SDR," in *Proc. 15th Int. Conf. Adv. Technol., Syst. Services Telecommun. (TELSIKS)*, Oct. 2021, pp. 41–44.

[20] L. Novosel and G. Sisul, "Chaotic direct sequence spread spectrum software defined radio system model using LabView," in *Proc. Int. Symp. ELMAR*, Sep. 2016, pp. 257–260.

[21] F. Rochim, "SCA system (subsidiary communications authorization) implementation of text transmission on broadcasting system," in *Proc. ICICI*, 2005, pp. 4–5.

[22] C. C. Do and H. H. Szu, "Video compression transmission via FM radio," *Proc. SPIE*, vol. 4391, pp. 455–464, Mar. 2001.

[23] A. L. Perrone and G. Basti, "RF video transmission," in *Proc. Int. Joint Conf. Neural Netw. (IJCNN)*, May 2002, pp. 2219–2224.

[24] (Apr. 9, 1998). *United States RBDS Standard*. Accessed: Jan. 7, 2023. [Online]. Available: http://wiki.tuxempire.de/images/6/65/Rbds1998.pdf

[25] M. Takada, T. Kuroda, and O. Yamada, "FM multiplex broadcasting system 'DARC,'" in *Proc. VNIS Vehicle Navigat. Inf. Syst. Conf.*, 1994, pp. 111–116, doi: 10.1109/VNIS.1994.396754.

[26] R. W. Stewart, K. W. Barlee, and D. S. Atkinson, *Software Defined Radio Using MATLAB & Simulink and the RTL-SDR*. New York. NY, USA: Strathclyde Academic Media, 2015.

[27] R. W. Stewart, "A low-cost desktop software defined radio design environment using MATLAB, simulink, and the RTL-SDR," *IEEE Commun. Mag.*, vol. 53, no. 9, pp. 64–71, Sep. 2015, doi: 10.1109/MCOM.2015.7263347.

[28] Z. Mahtab, S. J. Ahmed, S. S. Hussain, and S. Hasan, "CDMA based wireless transceiver system MATLAB simulation and FPGA implementation," in *Proc. Student Conf. Eng. Sci. Technol.*, Aug. 2005, pp. 1–9.
[29] R. M. Rao and S. A. Dianat, *Basics of Code Division Multiple Access (CDMA)*, vol. 67. Bellingham, WA, USA: SPIE, 2005.
[30] D. A. Guimaraes, *Digital Transmission: A Simulation-Aided Introduction With VisSim/Commun*. Cham, Switzerland: Springer, 2010.
[31] R. Keim. (Aug. 22, 2016). *Learning About Differential Quadrature Phase Shift Keying (DQPSK) Modulation*. Accessed: Jan. 7, 2023. https://www.allaboutcircuits.com/technical-articles/differential-quadrature-phase-shift-keying-dqpsk-modulation/
[32] F. J. MacWilliams and N. J. A. Sloane, "Pseudo-random sequences and arrays," *Proc. IEEE*, vol. 64, no. 12, pp. 1715–1729, Dec. 1976.
[33] A. Hightman, E. Chung, and A. Galvan. (Dec. 19, 2011). *CDMA Simulation*. Accessed: Jan. 2023. [Online]. Available: http://cnx.org/content/col11388/1.1/
[34] (Oct. 22, 1988). *Federal Communications Commission*. Accessed: Jan. 7, 2023. [Online]. Available: https://www.fcc.gov/media/radio/subcarriers-sca
[35] M. Zoltowski, "Equations for the raised cosine and square-root raised cosine shapes," *Commun. Syst. Division*, 2013.
[36] N. Srisakthi, C. V. R. Rao, and M. Vidya, "Implementation of CDMA receiver using recursive digital matched filter," *IOSR J. VLSI Signal Process.*, vol. 4, no. 3, pp. 23–28, 2014.
[37] Y. Wan and Z. Chen, "A novel synchronization method for DS-CDMA systems," in *Proc. 8th Int. Wireless Commun. Mobile Comput. Conf. (IWCMC)*, Aug. 2012, pp. 596–601.
[38] B. Sklar, *Digital Communications*, vol. 2. Upper Saddle River, NJ, USA: Prentice hall, 2001.
[39] *RDS/RBDS and RadioText Plus (RT+) FM Receiver. MATLAB*. Accessed: Jan. 7, 2023. [Online]. Available: https://www.mathworks.com/help/comm/ug/rds-rbds-and-radiotext-plus-rt-fm-receiver.html
[40] H. Osborne, "A generalized 'polarity-type' Costas loop for tracking MPSK signals," *IEEE Trans. Commun.*, vol. COM-30, no. 10, pp. 2289–2296, Oct. 1982, doi: 10.1109/TCOM.1982.1095399.
[41] M. Tytgat, M. Steyaert, and P. Reynaert, "Time domain model for Costas loop based QPSK receiver," in *Proc. PRIME 8th Conf. Ph.D. Res. Microelectron. Electron.*, 2012, pp. 1–4.
[42] W. A. Mahmoud Al-Jouher, J. M. A. Al-Samarei, and H. N. Abdullah, "Simulation of a DS/SS system using MATLAB-Simulink," *J. Eng. Develop.*, vol. 8, no. 3, pp. 42–58, Dec. 2004.
[43] Universal Software Radio Peripheral. *Ettus Research*. Accessed: Jan. 7, 2023. [Online]. Available: https://www.ettus.com/all-products/un210-kit/

RADU GABRIEL BOZOMITU (Member, IEEE) was born in Iaşi, Romania, in 1971. He received the degree in electronic engineering and communications, the master's degree in digital radio-communications, and the Ph.D. degree in electronics and telecommunications from the Faculty of Electronics, Telecommunications and Information Technology, "Gheorghe Asachi" Technical University of Iaşi, in 1995, 1996, and 2005, respectively. In 1998, he joined the Faculty of Electronics, Telecommunications and Information Technology, Department of Telecommunications and Information Technologies, "Gheorghe Asachi" Technical University of Iaşi, and received the title of a Professor, in 2017. In 2020, he became the Vice-Dean of the Faculty. He is the author of five books and more than 125 articles. His current research interests include the areas of radio communications, analog integrated circuit design, signal processing, and assistive technology. Courses taught at the "Gheorghe Asachi" Technical University of Iaşi are "radio communications," "VLSI implementation of the radiofrequency circuits," "advanced radio communications," and "software-defined radio."

FLORIN DORU HUTU (Senior Member, IEEE) was born in Iaşi, Romania, in 1979. He received the Engineering degree in electronics and telecommunications and the master's degree in digital radio-communications from the Faculty of Electronics, Telecommunications and Information Technology, "Gheorghe Asachi" Technical University of Iaşi, in 2003 and 2004, respectively, and the Ph.D. degree in automatic control from the University of Poitiers, France, in 2007.

He was a Postdoctoral Researcher at the XLIM Laboratory, for a period of two years. In September 2010, he became an Associate Professor at INSA Lyon, France, and he joined the INSA Lyon's Electrical Engineering Department and the INRIA's Socrate Team, CITI Laboratory. He is the author of more than 80 national and international scientific papers. His research interests include the energy efficient radio communications (wake-up radio, energy harvesting, and wireless power transfer) and RFID technologies. He is also involved in the design of software-defined radio architectures for the IoT.